

Prospects for natural SUSY

J. S. Kim*

Instituto de Física Teórica UAM/CSIC, Madrid, Spain

K. Rolbieceki†

Institute of Theoretical Physics, University of Warsaw, Poland

R. Ruiz‡

Instituto de Física Corpuscular, IFIC-UV/CSIC, Valencia, Spain

J. Tattersall§ and T. Weber¶

Institute for Theoretical Particle Physics and Cosmology, RWTH Aachen, Germany

As we anticipate the first results of the 2016 run, we assess the discovery potential of the LHC to “natural supersymmetry”. To begin with, we explore the region of the model parameter space that can be excluded with various centre-of-mass energies (13 TeV and 14 TeV) and different luminosities (20 fb^{-1} , 100 fb^{-1} , 300 fb^{-1} and 3000 fb^{-1}). We find that the bounds at 95% C.L. on stops vary from $m_{\tilde{t}_1} \gtrsim 800 \text{ GeV}$ expected this summer to $m_{\tilde{t}_1} \gtrsim 1500 \text{ GeV}$ at the end of the high luminosity run, while gluino bounds are expected to range from $m_{\tilde{g}} \gtrsim 1700 \text{ GeV}$ to $m_{\tilde{g}} \gtrsim 2500 \text{ GeV}$ over the same time period. However, more pessimistically, we find that if no signal begins to appear this summer, only a very small region of parameter space can be discovered with 5σ significance. For this conclusion to change, we find that both theoretical and systematic uncertainties will need to be significantly reduced.

I. INTRODUCTION

The Large Hadron Collider (LHC) has entered the next stage of its endeavour to discover physics beyond the standard model (BSM). Unfortunately, the lack of a clear signal of new physics has already significantly constrained the allowed parameter space of many BSM models. In particular, the limits on supersymmetric (SUSY) particles have moved, in many cases, well beyond 1 TeV (see e.g. [1–6]).

The improved limits on SUSY seem to be particularly damaging for constrained models that only have a few free parameters and do not offer much flexibility in the resulting mass spectra [7]. In addition, the heavy particles deduced from the limits threaten one of the main motivations for SUSY, which is stabilisation of the electroweak symmetry breaking scale (EWSB). However, the constrained models rely on assumptions about the details of the unknown SUSY breaking mechanism. Once we relax the assumptions about the high energy completion of the theory, the parameter space opens up to many new possibilities that could accommodate relatively light, but still not excluded, particles, while addressing some of the problems related to the naturalness of EWSB.

It has been noted [8–12] that for a successful stabilisation of the electroweak scale, only a small subset of

the many SUSY states are required to be light, and consequently, this helps to relax the general bounds on SUSY models with relatively light spectra. Such observations have renewed interest in so-called “natural supersymmetry” models in the context of LHC searches. The motivation behind natural supersymmetry is the question of fine-tuning, see e.g. [13, 14], which is required to obtain the desired scale of EWSB. Low fine-tuning demands certain parameters to be of order of the EWSB scale, in particular, the supersymmetric partners of the top quarks and Higgs bosons are expected to be light. A detailed analysis also reveals [15] that the amount of fine-tuning is closely related to the mass of the gluino, the superpartner of the gluon. Thus, within the naturalness paradigm, one can expect that SUSY is within the LHC reach, and many studies have investigated the phenomenology of natural SUSY at the LHC (see e.g. [10, 16–22]). On the other hand, the measured mass of the Higgs boson [23] requires rather heavy partners of top quarks [24] in the minimal supersymmetric standard model (MSSM) which clearly already puts the naturalness paradigm into question.

In Ref. [22] the authors presented constraints on a natural supersymmetry scenario derived from Run 1 results at the LHC. They called their scenario the minimal “natural supersymmetry”, since only the superparticles which were required to cancel the leading quadratically divergent corrections to the standard model (SM) Higgs mass were kept light. They derived robust limits, implying that the lighter stop mass eigenstate with mass below 230 GeV or a gluino with mass below 440 GeV is always excluded.

A dedicated analysis targeting natural SUSY was

* jong.kim@csic.es

† krolb@fuw.edu.pl

‡ rruiz@ific.uv.es

§ tattersall@physik.rwth-aachen.de

¶ torsten.weber@rwth-aachen.de

carried out by ATLAS in Ref. [3]. It resulted in rather weak limits, both in the simplified model setup and in a natural-supersymmetry-motivated phenomenological MSSM in a three-dimensional parameter space. The excluded stop masses were typically in the range 350–500 GeV, when the higgsino mass $\lesssim 150$ GeV. If simultaneous production of stops and sbottoms was taken into account, stop masses up to 680 GeV were excluded for higgsinos at the current limit ~ 100 GeV.

In this paper we revisit prospects for discovery of natural SUSY in the Run 2 of the LHC as well as after the future high luminosity (HL) upgrade. We follow a staged approach, which means that we consider different integrated luminosities and centre-of-mass energies that are currently planned at CERN [25, 26]:

- 13 TeV, 20 fb $^{-1}$ – expected for 2016;
- 13 TeV, 100 fb $^{-1}$ – Run 2 total luminosity by 2018;
- 14 TeV, 300 fb $^{-1}$ – Run 3 luminosity, 2020–2023;
- 14 TeV, 3000 fb $^{-1}$ – HL upgrade.

For each stage we analyse the expected exclusion limits, and in the case of the high luminosity upgrade we also consider the discovery reach for natural SUSY.

One of the main motivations of the current study is the question of what the potential future discovery reach is with increased centre-of-mass energy and integrated luminosity assuming that no signal is observed this year after collecting 20–30 fb $^{-1}$ of data. This is a relevant issue since 95% confidence level (C.L.) exclusion limits advance much faster than the discovery reach that conservatively requires 5σ significance for serious consideration. Therefore, if null results are obtained this year, the question is, can we still hope to make a discovery at the LHC? We find that the answer has a significant dependence on how well systematic uncertainties can be reduced in the future and we therefore consider different scenarios for their future evolution.

In this study we closely follow the numerical procedure of Ref. [22]. We investigate the minimal six-dimensional natural SUSY model where higgsinos, gluinos and third-generation squarks are all assumed to be in the vicinity of the TeV scale. We work within the MSSM setup, with the lightest neutralino as the lightest supersymmetric particle (LSP) assuming conserved R -parity [27]. We have randomly generated 20000 benchmark points in the minimal natural supersymmetry parameter space. The numerical analysis is performed with simulated Monte Carlo (MC) samples further processed by **CheckMATE** [28] using **Delphes** [29] for detector simulation and analysis. We include several ATLAS searches that are suited particularly well for natural SUSY, both inclusive and more specific for this model. The searches were optimised for different stages of the LHC operation from low to

high luminosities and an increased centre-of-mass energy.

The remainder of this article is organised as follows. In Sec. II we describe our natural SUSY inspired scenario and its collider signatures. Next, in Sec. III, we first discuss the numerical tools employed for this study and then discuss the setup for our scan. Finally, we present our numerical results in Sec. IV and show limits on the stop and the gluino mass as a function of the LSP mass. We conclude in Sec. V.

II. NATURAL SUPERSYMMETRY SETUP

The electroweak symmetry breaking condition of the MSSM dictates the following relation,

$$\mu^2 = \frac{m_{H_d}^2 - m_{H_u}^2 \tan^2 \beta}{\tan^2 \beta - 1} - \frac{1}{2} M_Z^2, \quad (1)$$

which correlates the supersymmetric Higgs mixing parameter μ with the soft supersymmetry breaking mass terms $m_{H_d}^2$ and $m_{H_u}^2$, the ratio of the two Higgs vacuum expectation values $\tan \beta = \frac{v_u}{v_d}$ and the observed Z mass. This tree level equation serves as the starting point for a qualitative discussion of naturalness. We regard the MSSM as natural if the individual terms are of the same order as M_Z . If the supersymmetric particles are too heavy, they will give large contributions to the various mass terms of Eq. (1). As a consequence, all individual contributions have to be finely tuned in order to obtain the correct Z boson mass.

However, not all supersymmetric sparticles contribute equally to Eq. (1). The most important contribution comes from the left-hand side, i.e., the μ parameter. Hence, a very simple definition of naturalness only requires the μ parameter to be of the order of the electroweak scale, and consequently, this implies light higgsinos [10, 11]. For example, the MSSM with $|\mu| \leq M_Z$ would be regarded as *very* natural, although this is already in conflict with the LEP2 results [30]. Recently, it has been pointed out that an exception to this rule is possible if an additional Higgsino soft breaking term is included [31], and this allows for $m_{\tilde{H}} \lesssim 500$ GeV for $\sim 10\%$ tuning.

Unfortunately, radiative corrections complicate this picture significantly and must be included for consistency since they can lead to very large effects. The dominant one-loop corrections to $m_{H_u}^2$ and $m_{H_d}^2$ in Eq. (1) are driven by the top partners (stops) since they couple with the large top Yukawa coupling strength. As the one-loop contribution scales with the square of the stop masses, the stops should not be too heavy ($m_{\tilde{t}} \lesssim 800$ GeV for $\sim 10\%$ tuning [12]) in order to prevent unduly large contributions to the right-hand side of Eq. (1). Analogously, two-loop corrections renormalise the Higgs soft breaking masses as well and put an upper limit on the gluino mass ($m_{\tilde{g}} \lesssim 1200$ GeV for $\sim 10\%$ tuning [12]), though the

constraints are weaker than those present on the higgsino and stop mass. The following qualitative picture emerges from the naturalness principle: light higgsinos, not too heavy stops and gluinos that are not decoupled from the LHC phenomenology [8, 9, 12].

However, the exact definition of naturalness depends on the degree of fine-tuning. A quantitative measure of fine-tuning was defined in [13]:

$$\Delta = \left| \frac{a}{M_Z^2} \frac{\partial M_Z^2}{\partial a} \right|, \quad (2)$$

where a is an input parameter which can be a soft breaking parameter at the electroweak scale, but it could equally well be a universal soft breaking parameter at some high scale of a constrained supersymmetric model. A value of $\Delta = 20$ would then correspond to a fine-tuning of $\Delta^{-1} = 5\%$. Equation (2) together with the amount of fine-tuning Δ that one is willing to accept, gives an upper limit on the sparticle masses. Due to their much smaller couplings, it is clear that the first two generation squarks and sleptons, as well as the electroweak bino and wino, only have a negligible impact on naturalness.

Here, we want to be agnostic about the exact amount of *natural* fine-tuning, since this is somewhat subjective. We closely follow the description of the natural SUSY particle spectrum discussed in Ref. [22]. We only consider supersymmetric particles which are essential to cancel the quadratic divergences to the Higgs mass, and thus our scenario can be regarded as the minimal natural MSSM. We demand higgsinos with masses below the TeV scale, third-generation soft squark masses up to 2 TeV and gluinos with masses below 3 TeV. We assume that all sleptons and the first- and second-generation squarks have a common mass scale at $m_{\tilde{f}}^2 = 1.5 \times 10^7 \text{ GeV}^2$. Since we only consider scenarios with $\tan \beta \leq 20$, the sbottom loop contribution to the Higgs mass is negligible, and thus we fix the mass of the right-handed sbottom b_R at the same common sfermion mass scale $m_{\tilde{f}}$. However, since we consider both stop states, in particular, the SU(2)-doublet stop, we also have to include the left-handed sbottom due to weak isospin invariance. A_b does not play a role in the phenomenology, and we fix it to $A_b = 0 \text{ GeV}$ without loss of generality. Finally, we set the bino mass parameter M_1 and wino mass parameter M_2 to 3 TeV. All additional MSSM Higgs bosons are assumed to be decoupled by fixing the pseudoscalar mass at $m_A = 2.5 \text{ TeV}$. Figure 1 shows the supersymmetric particle spectrum of the minimal natural MSSM. In summary, our natural SUSY scenario is parametrised in terms of six parameters: the supersymmetric Higgs mixing parameter μ , the gluino mass parameter M_3 , $\tan \beta$, the third-generation SU(2)-doublet squark soft-breaking parameter m_{Q_t} , the corresponding SU(2)-singlet soft-breaking parameter m_{t_R} , and the top trilinear soft-breaking term A_t .

In natural SUSY the dominant production mechanism is the pair production of third-generation sparti-

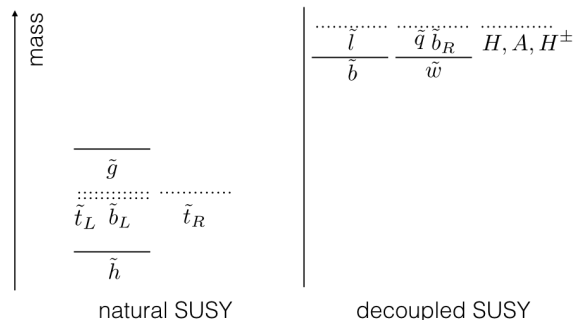


FIG. 1. The minimal natural SUSY mass spectrum are shown on the left, while the remaining supersymmetric particles are decoupled on the right.

cles and gluinos via strong interactions,

$$pp \rightarrow \tilde{g}\tilde{g}, \quad pp \rightarrow \tilde{t}_{1(2)}\tilde{t}_{1(2)}^*, \quad pp \rightarrow \tilde{b}_1\tilde{b}_1^*. \quad (3)$$

Here, we will not consider direct higgsino pair production. In general, the mass splitting between the higgsino mass eigenstates is a few GeV, and thus the energy release of the SM particles in $\tilde{\chi}_1^\pm$ and $\tilde{\chi}_2^0$ decays is too small to be detected at the LHC. Both are invisible at the LHC provided their decays into the $\tilde{\chi}_1^0$ LSP are prompt. As a result, only higgsino pair production in association with a jet yields a viable collider signature. However, the small production cross section for the monojet final state, together with the large systematic uncertainty of the SM background prediction,¹ allows only the exclusion of very light higgsinos even at the high luminosity phase of the LHC [33].

The decay modes of the coloured sparticles are complicated and depend on the mass hierarchy as well as the mixing of the third-generation sparticles. If the gluino is decoupled, the following third-generation scalar decays can occur,

$$\tilde{t}_a \rightarrow t\tilde{\chi}_l^0, \quad b\tilde{\chi}_1^\pm, \quad l = 1, 2, \quad (4)$$

$$\tilde{b}_1 \rightarrow b\tilde{\chi}_l^0, \quad t\tilde{\chi}_1^\pm, \quad l = 1, 2. \quad (5)$$

When we neglect phase-space suppression, the branching ratios of the stops are determined by the dominant coupling character of the state in question. Namely, the SU(2)-doublet decays mainly to $t\tilde{\chi}_{1,2}^0$ since the $\tilde{t}_L t \tilde{\chi}_{1,2}^0$ coupling is proportional to the top Yukawa coupling, while $\tilde{t}_L b \tilde{\chi}_1^\pm \sim Y_b$ in the higgsino case. On the other hand, the SU(2)-singlet \tilde{t}_1 decays to $b\tilde{\chi}_1^\pm$ and $t\tilde{\chi}_{1,2}^0$ at similar rates, with all couplings proportional to Y_t for higgsinos (see e.g. [34]).

¹ For a discussion of the systematic uncertainty, please refer to the discussion in Ref. [32]

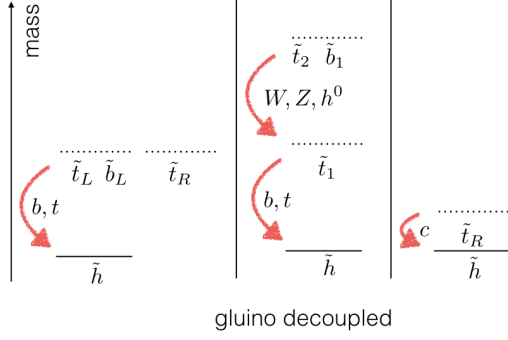


FIG. 2. Decay modes in natural SUSY assuming decoupled gluinos.

Decays into lighter third-generation scalars involving SM gauge bosons and the Higgs scalar are also possible,

$$\tilde{t}_a \rightarrow \tilde{b}_1 W^\pm, \quad \tilde{b}_1 \rightarrow \tilde{t}_1 W^\pm, \quad (6)$$

$$\tilde{t}_2 \rightarrow \tilde{t}_1 Z, \quad \tilde{t}_2 \rightarrow \tilde{t}_1 h. \quad (7)$$

If the two-body decay modes are kinematically closed, in particular, $\tilde{t}_1 \rightarrow b\tilde{\chi}_1^\pm$, the stop can have a sizeable branching ratio in three- and four-body final states. If all tree-level decays of the lighter stop \tilde{t}_1 are heavily suppressed, the loop-induced decay $\tilde{t}_1 \rightarrow c\tilde{\chi}_1^0$ can be the dominant decay mode of the lighter stop [35]. Examples of a typical spectrum in the gluino decoupled case with the corresponding decay modes are shown in Fig. 2.

If the gluino is light enough, direct decays of the third-generation particles via strong interactions are possible,

$$\tilde{t}_a \rightarrow t\tilde{g}, \quad \tilde{b}_1 \rightarrow b\tilde{g}, \quad a = 1, 2. \quad (8)$$

However, in this region of parameter space the far larger gluino production rate means that the production of the heavier stops is phenomenologically unimportant.

Finally, gluinos typically decay via

$$\tilde{g} \rightarrow \tilde{t}_a \bar{t}, \quad \tilde{t}_a^* t, \quad \tilde{b}_1 \bar{b}, \quad \tilde{b}_1^* b, \quad a = 1, 2. \quad (9)$$

If the two-body decays are phase-space suppressed, decays via off-shell squarks are possible,

$$\tilde{g} \rightarrow t\bar{t}\tilde{\chi}_{1(2)}^0, \quad b\bar{b}\tilde{\chi}_{1(2)}^0, \quad \bar{t}b\tilde{\chi}_1^+, \quad \bar{b}t\tilde{\chi}_1^-. \quad (10)$$

We can already see that the gluino pair production will yield high b -jet multiplicities in the final state. If all third-generation particles are decoupled, the loop-induced decay can become dominant [36],

$$\tilde{g} \rightarrow g\tilde{\chi}_1^0. \quad (11)$$

Several characteristic decay modes with sample mass hierarchies are summarised in Fig. 3.

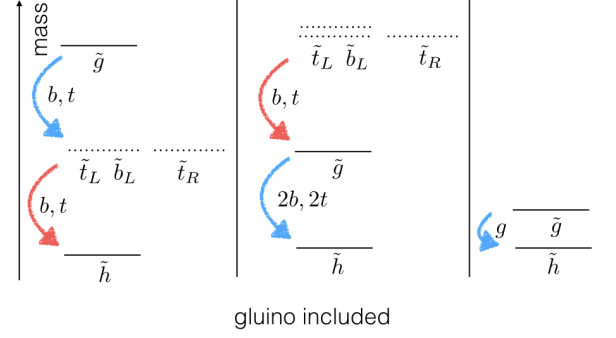


FIG. 3. Decay modes in natural SUSY assuming light gluinos in the spectrum.

III. NUMERICAL ANALYSIS

A. Numerical tools

The masses, couplings and branching ratios of all sparticles in our natural SUSY setup are calculated with **SPheno** 3.2.4 [37].² For each model point, MC events are generated with **Pythia** 8.210 [38, 39] at the centre-of-mass energy 14 TeV using its default parton distribution function set [40]. The production cross sections are normalised with **NLLFAST** 4.1 [41–46], which computes hadronic SUSY cross sections at next-to-leading order and resums the soft gluon emission at next-to-leading logarithmic accuracy. The hadronic events have been passed to **CheckMATE** 1.2.1 [28, 47, 48], which is based on the fast detector simulation **Delphes** 3.10 [29] and **Fastjet** 3.0.6 for the jet reconstruction [49–51]. **CheckMATE** tests all model points against experimental searches at the LHC. For each model point, it determines the number of expected signal events in all signal regions. In order to test the future exclusion sensitivity and discovery potential, we compare the signal predictions with the SM background estimates and errors provided by the ATLAS Collaboration for a given luminosity and centre-of-mass energy. In order to make predictions at other energies or total integrated luminosities, the background numbers and errors have to be rescaled accordingly. The precise procedure we use is described in Sec. III C.

B. Scan procedure

We have randomly generated numerical values for the natural SUSY parameters listed together with

² For the Higgs mass constraint we use **SPheno** 3.3.8.

their scan ranges:

$$\begin{aligned}
0.1 \text{ TeV} &\leq |\mu| \leq 1.0 \text{ TeV}, \\
0.1 \text{ TeV} &\leq m_{\tilde{Q}_t} \leq 2.0 \text{ TeV}, \\
0.1 \text{ TeV} &\leq m_{\tilde{t}_R} \leq 2.0 \text{ TeV}, \\
0.1 \text{ TeV} &\leq |M_3| \leq 3.0 \text{ TeV}, \\
|A_t| &\leq 3.0 \text{ TeV}, \\
1 &\leq \tan \beta \leq 20.
\end{aligned}$$

All probability distribution functions for the input parameters are flat, and their lower limits are motivated by the null results from searches for supersymmetric particles performed by the LEP2 and Tevatron experiments.

The soft breaking parameters are given in the $\overline{\text{DR}}$ scheme and passed to the spectrum generator **SPheno**, which calculates on-shell masses and decay widths as well as low-energy electroweak precision observables. We apply a large number of theoretical and experimental constraints on our benchmark points, which we will discuss in the following.

We demand that all benchmark points satisfy the conditions for correct electroweak symmetry breaking and that the spectrum is tachyon free. Moreover, we demand a CP-even Higgs boson with a mass $m_h = 125 \pm 3$ GeV with SM-like couplings. We also test our benchmark points against electroweak precision observables such as the ρ parameter [52] and constraints from b physics experiments [53]. In particular, we take into account constraints from $b \rightarrow s\gamma$, $b \rightarrow s\mu^+\mu^-$ and $B_u \rightarrow \tau\nu$. We apply a lower limit on the chargino mass of 100 GeV [54–56]. Finally, we demand a sufficiently large mass splitting, $m_{\tilde{\chi}_1^\pm} - m_{\tilde{\chi}_1^0} > 280$ MeV, between the higgsino-like NLSP ($\tilde{\chi}_2^0, \tilde{\chi}_1^\pm$) and the LSP ($\tilde{\chi}_1^0$), allowing for a prompt decay, so we do not consider searches for long-lived SUSY particles.

Since R -parity is conserved, the LSP is stable and contributes to the dark matter relic density. For standard cosmology scenarios, the abundance is determined by the thermally averaged annihilation cross section, and the resulting relic density has to satisfy the precision measurement of the dark matter density from the cosmic microwave background. However, a higgsino dark matter particle efficiently annihilates into SM particles and satisfies the upper limit on the relic density unless $m_{\tilde{\chi}_1^0} \gtrsim 1$ TeV [57], which is satisfied by all of our points. In addition, if we extended our minimal natural SUSY scenario with a bino-like neutralino LSP or a singlino LSP, the observed dark matter abundance could be explained in a large region of our parameter space [58, 59].

From the 150000 benchmark points initially generated, 20000 pass all preselection cuts. We show in Fig. 4 the distributions of the higgsino, third-generation scalar quark and gluino masses. The higgsino is the lightest sparticle in our spectrum and has a reasonably flat mass distribution. However, it decreases at its upper limit since in this region of pa-

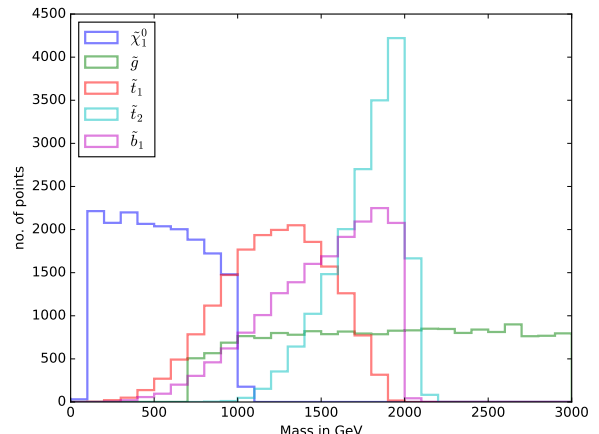


FIG. 4. Distributions for the masses of the SUSY particles, $\tilde{\chi}_1^0$, \tilde{g} , \tilde{t}_1 , \tilde{t}_2 and \tilde{b}_1 , for our model points satisfying the preselection criteria.

rameter space the higgsino is quite often not the LSP, consequently, these benchmark points are removed.

Only a few benchmark points contain a very light stop with masses below 500 GeV. A light \tilde{t}_1 usually requires a heavy \tilde{t}_2 in order to increase the Higgs mass sufficiently. This can be seen in the rather large mass splitting between the lighter and heavier stop mass eigenstates. The direct stop searches of Run 1 are not sensitive to \tilde{t}_2 production for our parameter points since the cross section is too small, although indirect production via gluino decay may still be a non-negligible production channel. However, for Run 2 and for larger integrated luminosities, direct \tilde{t}_2 pair production may become accessible at the LHC.

For the sbottom mass eigenstate \tilde{b}_1 , the distribution covers a large range of masses. An $\text{SU}(2)$ -doublet stop is accompanied by a sbottom with similar mass, and thus we expect for light left-handed stops, light sbottoms in the mass spectrum as well. The gluino mass distribution is flat above 1 TeV. It quickly falls off for gluino masses below 1 TeV since here the gluino could become lighter than the higgsino; hence these points would be removed.

Table I shows all relevant searches currently implemented in **CheckMATE** and the left column provides the **CheckMATE** identifier for each search. The second column gives the centre of mass energy and the third column displays the integrated luminosity that the search has originally been tuned for, and the fourth column gives the target final state for which the corresponding search has been optimised for. The majority of the implemented searches are official ATLAS high luminosity studies which already cover a large number of our final state topologies. However, since we expect a large b -jet multiplicity in our natural SUSY scenarios, we have also included the current multi- b -jet and missing transverse momentum search at $\sqrt{s} = 13$ TeV with a

total integrated luminosity of 3.3 fb^{-1} [60]. Detailed information about the implemented searches can be found in Sec. III D.

The calculation procedure starts with the generation of Monte Carlo events, including all hadronic production processes given in Eq. (3). The relative frequency of MC events is weighted according to the NLO+NLL cross section of the respective production channel. The hadronic MC events are then passed to **CheckMATE** which simulates the ATLAS detector response with the fast detector simulation **Delphes** which has a modified detector tuning and an extended list of final state objects. In particular, realistic b -jet tagging efficiencies and mistagging efficiencies were implemented. This is essential to obtain reliable results since a large number of natural SUSY searches in Table I rely on b -tagging in order to isolate the signal from SM backgrounds. **CheckMATE** further processes the reconstructed detector-level objects with its analysis module.

All searches listed in Table I have been carefully implemented and validated, and detailed information on the validation can be found on the official **CheckMATE** web page [48]. Each model point was tested against all the analyses given in Table I. To do this, **CheckMATE** calculates the efficiencies for all signal regions of all employed searches, and the program then chooses the signal region with the most sensitivity. To determine whether the model point in question is excluded at the 95% C.L. [61], we evaluate the ratio

$$r \equiv \frac{S - 1.96 \cdot \Delta S}{S_{\text{exp.}}^{95}}, \quad (12)$$

where S is the number of expected signal events, ΔS denotes its theoretical uncertainty, and $S_{\text{exp.}}^{95}$ is the theoretically determined 95% C.L. limit on the signal depending on the number of background events and its statistical as well as systematic error. **CheckMATE** does not statistically combine signal regions of all the employed ATLAS searches. We consider a model to be excluded at 95% C.L. if r defined in Eq. (12) exceeds 1.

In addition, we also display points that are confidently allowed at a certain energy and luminosity. Here we use an adjusted r' value, given as

$$r' \equiv \frac{S + 1.96 \cdot \Delta S}{S_{\text{exp.}}^{95}}, \quad (13)$$

and define the point as allowed if $r' < 1$. Finally, we define points as “ambiguous” if neither of the above conditions are met.

In this work we are also interested in the discovery potential, and for this calculation we adopt the method called Z_{Bi} in Ref. [62] due to its optimality properties. The algorithm incorporates uncertainties in the background estimation in a fully frequentist fashion.

C. Rescaling due to energy and luminosity

To be able to investigate all the combinations of centre-of-mass energy and integrated luminosity described above, a rescaling procedure has been used. We use a rescaling since there are currently only a handful of searches published by the ATLAS and CMS collaborations that target relevant processes at the high luminosity LHC. After trying to fully reproduce all significant standard model and detector backgrounds, we found that such a rescaling is more accurate than, for example, trying to reproduce the correct multi-jet background estimation using a fast detector simulation.

All the searches used are listed in Table I. We can see that most analyses are for 14 TeV and 3000 fb^{-1} and no analyses are available for 13 TeV and 20 fb^{-1} or 100 fb^{-1} . Since we want to compare the exclusion reach of the LHC at these various steps, we rescale the background numbers given by the original searches to the centre-of-mass energies and integrated luminosities that we need. We also rescale the generated signal events in the same way to correctly reproduce the signal-to-background ratio at different energies. The exact rescaling procedures are described below.

1. Rescaling the searches

We start the discussion with rescaling the searches to the different integrated luminosities and centre-of-mass energies considered. This method will later be used in **CheckMATE** to compute new $S_{\text{exp.}}^{95}$ values that are used to test model points. The calculation requires the number of expected background events and its uncertainty for each signal region. Two different rescaling procedures are used: one to change the centre-of-mass energy and the other to change the integrated luminosity.

a. Changing the centre of mass energy To change the centre-of-mass energy of a search, the number of background events and their uncertainties are rescaled with the ratio of the tree-level cross sections at the two centre-of-mass energies. The cross sections used for this rescaling were obtained using **MadGraph** [65, 66]. As a consequence, we assume that the ratio of the signal-to-background kinematic distributions will not change significantly between 13 TeV and 14 TeV, or at least similarly enough so that the signal regions defined by the searches are insensitive to the difference within errors.

To rescale the background numbers, every background process is scaled separately, and then all processes are summed to give the total number of background events at the new centre-of-mass energy. For some of the searches, background numbers are only listed for the most significant background processes. In that case the sum of the individual numbers of background events is not equal to the total number

| Analysis (CheckMATE identifier) | Energy (TeV) | Luminosity (fb ⁻¹) | Process targeted | Final state | Reference |
|------------------------------------|-----------------|-----------------------------------|--|--|-----------|
| atlas.conf_2015_067 | 13 | 3.3 | $\tilde{g}\tilde{g}$ | ≥ 3 b -jets + MET | [60] |
| atlas.phys_2014_010_300 | 14 | 300 | $\tilde{g}\tilde{g}, \tilde{q}\tilde{q}$ | 2-6 jets + MET | [63] |
| atlas.phys_2014_010_h1_3l | 14 | 3000 | $\tilde{\chi}_1^\pm \tilde{\chi}_2^0$ | 3 leptons + MET | [63] |
| atlas.phys_2014_010_sq_hl | 14 | 3000 | $\tilde{g}\tilde{g}, \tilde{q}\tilde{q}$ | 2-6 jets + MET | [63] |
| atlas.phys_pub_2013_011 | 14 | 3000 | $t\bar{t}$ | 0-1 lepton + ≥ 3 jets + ≥ 1 b -jet + MET | [64] |
| atl.phys_pub_2014_010_sbottom | 14 | 300 | $b\bar{b}$ | 2 b -jets + MET | [63] |

TABLE I. Summary of the analyses used to test models, along with the energy and luminosity that they have originally been optimised for.

of background events provided by the ATLAS note. When rescaling such a search, the relative difference between the total background and the sum of the individual processes is kept constant. The uncertainties on the backgrounds are scaled with the same factor as the corresponding background and are then combined in the same way as in the original study to give the total background uncertainty. Due to some of the searches missing background contributions and uncertainty correlations being taken into account, a simple combination is not always possible. To estimate these effects, we follow the same approach as for the total numbers and keep the relative difference between the total and the sum of the individual contributions constant.

b. Changing the integrated luminosity When changing the integrated luminosity from l_1 to l_2 , the number of background events and the uncertainty are scaled with the ratio l_2/l_1 . This assumes that nothing other than the number of expected events (signal or background) changes between the two luminosities, and for example, possible detector upgrades or differences in pileup are not taken into account.

2. Rescaling the signal events

When CheckMATE tests a parameter point against a particular analysis, it sums the weights of the generated signal events that fall into each signal region. To compare this number against the expected number of background events, CheckMATE normalises the weighted MC events to the cross section of the process and the integrated luminosity for the analysis. When rescaling the signal events, the same normalisation procedure is repeated with the desired integrated luminosity and with the cross section of the process at the desired centre-of-mass energy. As with the rescaled backgrounds, the effects of different acceptance times efficiency following from modified kinematical distributions at different centre-of-mass energies are neglected. Also, as for the backgrounds, different pileup and possible detector improvements for the various integrated luminosities are not taken into account. The uncertainties on both the number of signal events and on the cross section are normalised

using the same factor as for the signal events. Consequently, the relative uncertainties remain unchanged after rescaling.

3. Reduced systematic uncertainty scenario

To account for possible future improvements in the various systematic uncertainties, we also consider a scenario where these uncertainties are reduced with the integrated luminosity. In this case we fix the values of errors at 20 fb⁻¹ and then assume that the systematic uncertainties scale like a statistical error with added data; i.e., the relative uncertainty decreases with the square root of luminosity, $\propto 1/\sqrt{\mathcal{L}}$. This procedure is performed for the uncertainty on the number of background events and on the cross section. These uncertainties can be reasonably expected to improve in the coming years with a better understanding of the detectors resulting in reduced systematics and, from the theory side, with more precise calculations of the relevant background and signal processes. Additional improvements are expected for the parton distribution functions at the higher centre-of-mass energies probed now at the LHC.

Nevertheless, it is extremely hard to predict how these uncertainties will reduce in the coming years. We choose to reduce the errors as a statistical uncertainty since the dominant LHC paradigm is to normalise backgrounds with dedicated control regions and only use theoretical predictions to extrapolate these results into signal regions. Obviously, these extrapolations are independent of the collected statistics but can be improved beyond the naive theoretical uncertainty by combining the results of many different independent validation and control regions (especially for processes like $t\bar{t}$ production with many different final states to study). Any estimate is further complicated by the fact that there is a different proportion of background final states in each individual signal region we examine. In addition, each signal region probes a different amount into the tail of the corresponding background distribution.

In conclusion, to make a more thorough prediction of the background uncertainty would require a detailed analysis of each individual signal region. This would

entail a significant amount of work but would still be extremely speculative in nature. Therefore we believe that the far simpler and transparent procedure of simply reducing the uncertainty due to statistics is more sensible. This should be considered as the “most” optimistic scenario, and our opinion is that reality will lie somewhere between the two extremes presented.

Explicitly, the method we use is that the systematic uncertainties are first scaled linearly down to l_b from l_1 , where l_b is the base luminosity of 20 fb^{-1} and l_1 the original luminosity for a given search. The uncertainties are then scaled up to the new luminosity l_2 with $\sqrt{l_2/l_b}$, giving the complete expression as

$$\sigma'(l_2) = \frac{l_b}{l_1} \sqrt{\frac{l_2}{l_b}} \sigma(l_1), \quad (14)$$

where σ (σ') is either the original (rescaled) uncertainty on the number of background events or the uncertainty of the cross section. The above expression can be trivially rewritten as

$$\frac{\sigma'(l_2)}{l_2} = \sqrt{\frac{l_b}{l_2}} \frac{\sigma(l_1)}{l_1}, \quad (15)$$

which explicitly shows that the relative uncertainty scales as $1/\sqrt{\mathcal{L}}$.

D. Experimental analyses considered

The backbone of our study are the searches ATLAS proposed for HL-LHC analyses [63]. These analyses take into account the upgraded ATLAS detector configuration, HL-optimised selections and MC-derived estimation of background processes. They target the following SUSY benchmark processes:

- direct production of charginos and neutralinos with decays via W , Z , h ;
- production of squarks (1st and 2nd generation) and gluinos;
- production of bottom squarks.

The assumed centre-of-mass energy is 14 TeV, and the integrated luminosities of 300 fb^{-1} and 3000 fb^{-1} were considered. The searches have now been incorporated into **CheckMATE** and are summarised in Table I. Our validation was performed based on the information provided in Ref. [63], both for signal and background processes.

Since stop production is also clearly important in our natural SUSY scenario, we also include the separate high luminosity stop analysis [64]. This is also optimised for $\sqrt{s} = 14 \text{ TeV}$, with a final state containing several jets, at least one b -jet, 0–1 leptons and missing transverse energy; see Table I.

We also include a recent study searching for the direct production of gluinos, based on data collected

during the first phase of Run 2 in 2015. The study targets multi- b -jets final states with additional missing transverse energy. While it was optimised for low integrated luminosity, it may still be relevant for gluino exclusion when we consider prospects at 20 fb^{-1} and relatively light gluinos. We note here that the high luminosity analyses optimised for heavy SUSY particles could have a limited sensitivity for gluinos just above the current exclusion limits because the signal regions are tuned for higher mass states.

Finally, we also retest points that cannot be excluded with the above searches, with the full suite of **CheckMATE** analyses at 8 TeV. As will be seen in the results section, there are a few points containing light stops that the high energy analyses are insensitive to because they are tuned to higher mass SUSY production. However, these points are already excluded by 8 TeV searches [67–70].

IV. RESULTS

As described in the numerical analysis section, we study four different collider scenarios which reflect the expected progress of the LHC in the coming years. Namely, we consider 20 fb^{-1} and 100 fb^{-1} at 13 TeV, which is the current integrated luminosity estimate for Run 2 before the long shutdown begins in late 2018. We make the assumption that by 2021 the full capability of the LHC will be achieved, and the restart will be at 14 TeV. Here we study two integrated luminosity scenarios, 300 fb^{-1} and 3000 fb^{-1} .

A. Exclusion with 20 fb^{-1} at 13 TeV

To begin, we examine our baseline study of 20 fb^{-1} data collected at 13 TeV. If we look at Fig. 5 (left), we plot the excluded, ambiguous or allowed points in the $m_{\tilde{g}}$ vs $m_{\tilde{\chi}_1^0}$ plane in scenarios with $m_{\tilde{t}_1} > 1000 \text{ GeV}$. We remove scenarios with light \tilde{t}_1 states so that we can clearly see the dependence on the \tilde{g} mass. Once these points have been removed, we can very clearly see that the phenomenology of the model in this region of parameter space is dominated by the gluino and LSP masses. More precisely, we see that scenarios with gluino masses up to 1700 GeV can reliably be excluded if the parameter point contains relatively light LSP masses ($m_{\tilde{\chi}_1^0} < 600 \text{ GeV}$). Once the LSP mass becomes larger, however, for the compressed part of the spectra, $m_{\tilde{g}} - m_{\tilde{\chi}_1^0} \lesssim 300 \text{ GeV}$, the exclusion is no longer reliable. The lack of exclusion in compressed spectra is a well-known phenomenon that occurs because the decay products of the gluino become much softer and are thus harder to distinguish from the SM background [71–73]. The largest excluded LSP masses we find have $m_{\tilde{\chi}_1^0} \sim 1000 \text{ GeV}$ and are reached when $m_{\tilde{g}} \simeq 1500 \text{ GeV}$.

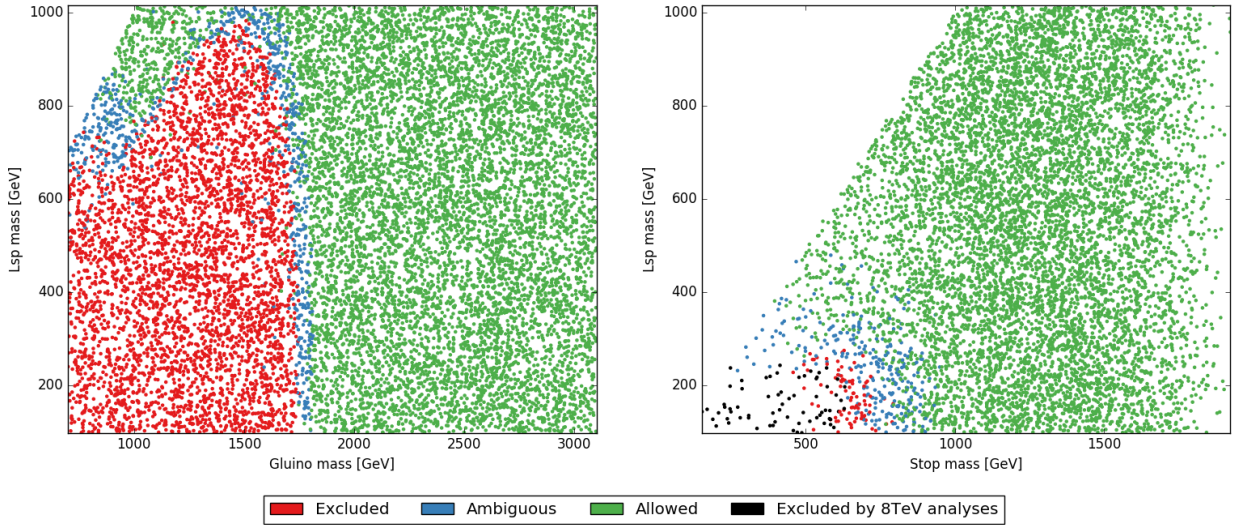


FIG. 5. Plots showing the natural SUSY points that are allowed, excluded or ambiguous within the Monte Carlo uncertainty at $\sqrt{s} = 13$ TeV with $\mathcal{L} = 20 \text{ fb}^{-1}$, under the assumption that the current systematic errors will remain constant. Left: $m_{\tilde{g}}$ vs $m_{\tilde{\chi}_1^0}$ for $m_{\tilde{t}_1} > 1000$ GeV. Right: $m_{\tilde{t}_1}$ vs $m_{\tilde{\chi}_1^0}$ for $m_{\tilde{g}} > 2000$ GeV.

We now move on to concentrate on the light \tilde{t}_1 scenarios that we have just projected out. To do this we plot in Fig. 5 (right) the excluded, ambiguous or allowed points in the $m_{\tilde{t}_1}$ vs $m_{\tilde{\chi}_1^0}$ plane in scenarios with $m_{\tilde{g}} > 2000$ GeV. The light gluino parameter points are removed for exactly the same reasoning as above so that we can concentrate on the light \tilde{t}_1 phenomenology. We find that for a light LSP ($m_{\tilde{\chi}_1^0} < 200$ GeV), stops can be excluded up to $m_{\tilde{t}_1} < 800$ GeV.

As for the gluino limits, we find that as the LSP becomes heavier ($m_{\tilde{\chi}_1^0} > 200$ GeV), the stop limits that we can set, quickly degrade. Again, the reason is that as the scenarios become compressed, the energy of the visible final state is significantly reduced and the analyses lose sensitivity [74–76]. As an extreme example, we find points with $m_{\tilde{t}_1} < 500$ GeV still allowed when $m_{\tilde{\chi}_1^0} \sim 300$ GeV. However, we want to point out that very long-lived stops could be observed at the LHC via R hadron searches [77, 78]. We also note that we found a large cluster of points at low stop mass that could not be excluded by the high energy searches that we used. However, the reason is not that these points cannot be excluded at 13 TeV with 20 fb^{-1} but rather that the searches we use have signal regions tuned for higher mass states. To illustrate our point, we retest all of the light points that cannot be excluded with the 8 TeV searches implemented in **CheckMATE** and these are given in black. Therefore, we see that the 8 TeV signal regions that have been tuned better for these stop masses successfully cover the low mass region.

B. Exclusion with 100 fb^{-1} at 13 TeV

If we stay at 13 TeV but now move to 100 fb^{-1} , we see that the exclusion bounds for both the gluino and stop increase but only by a small amount. More precisely, Fig. 6 shows that the exclusion on the gluino mass now reaches almost 2000 GeV while $m_{\tilde{t}_1} > 1200$ GeV. More important, however, is the observation that the number of compressed points that are definitely allowed is significantly reduced. If we make the assumption that searches will exist that target this region with specifically tuned cuts, the compressed region can be excluded up to $m_{\tilde{\chi}_1^0} \simeq 900$ GeV.

Moving on to the stop searches, we see a similar improvement. Parameter points with $m_{\tilde{t}_1} < 1000$ GeV are now regularly excluded, but we should also make it clear that some points are allowed even though they have $m_{\tilde{t}_1} \sim 900$ GeV and a light LSP with $m_{\tilde{\chi}_1^0} \sim 200$ GeV. Once again, we see a reduction in the limit as the LSP mass is increased. However, the light stop points ($\tilde{t}_1 < 500$ GeV) that were previously allowed with 20 fb^{-1} are now in the “ambiguous” region and could probably be excluded with targeted searches.

C. Exclusion with 300 fb^{-1} at 14 TeV

In Fig. 7 we display the points predicted for exclusion with 300 fb^{-1} at 14 TeV, and as expected, we see that the bounds further improve from those obtained at 13 TeV. For gluinos, assuming $m_{\tilde{t}_1} > 1300$ GeV, Fig. 7 (left), the exclusion in some parameter points extends to over $m_{\tilde{g}} \sim 2200$ GeV, and the exclusion is almost complete in the compressed region even as the LSP mass reaches $m_{\tilde{\chi}_1^0} \sim 1000$ GeV.

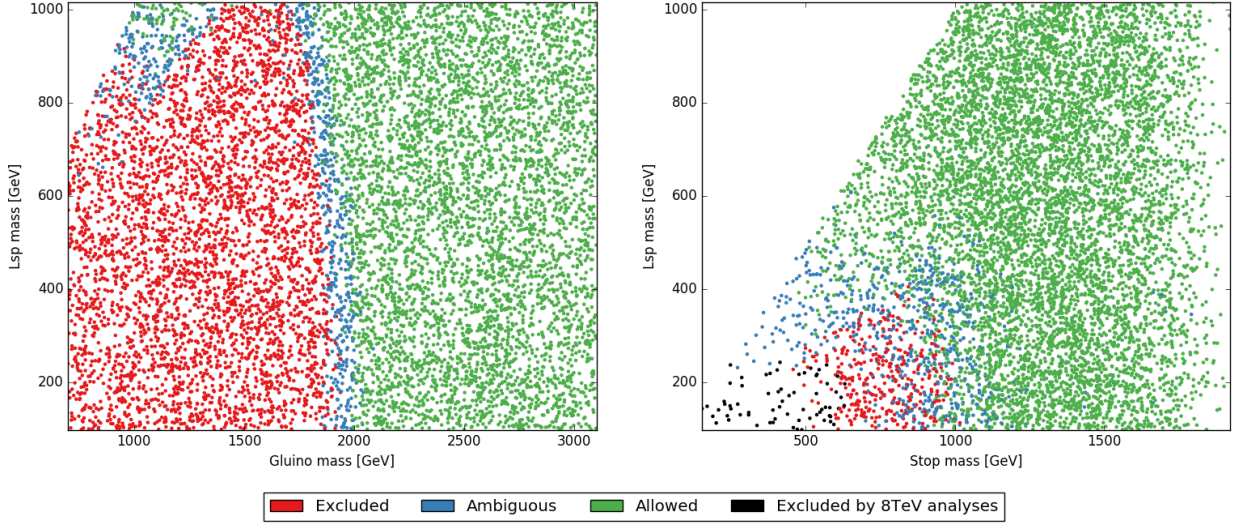


FIG. 6. Plots showing the natural SUSY points that are allowed, excluded or ambiguous within the Monte Carlo uncertainty at $\sqrt{s} = 13$ TeV with $\mathcal{L} = 100 \text{ fb}^{-1}$, under the assumption that the current systematic errors will remain constant. Left: $m_{\tilde{g}}$ vs $m_{\tilde{\chi}_1^0}$ for $m_{\tilde{t}_1} > 1200$ GeV. Right: $m_{\tilde{t}_1}$ vs $m_{\tilde{\chi}_1^0}$ for $m_{\tilde{g}} > 2000$ GeV.

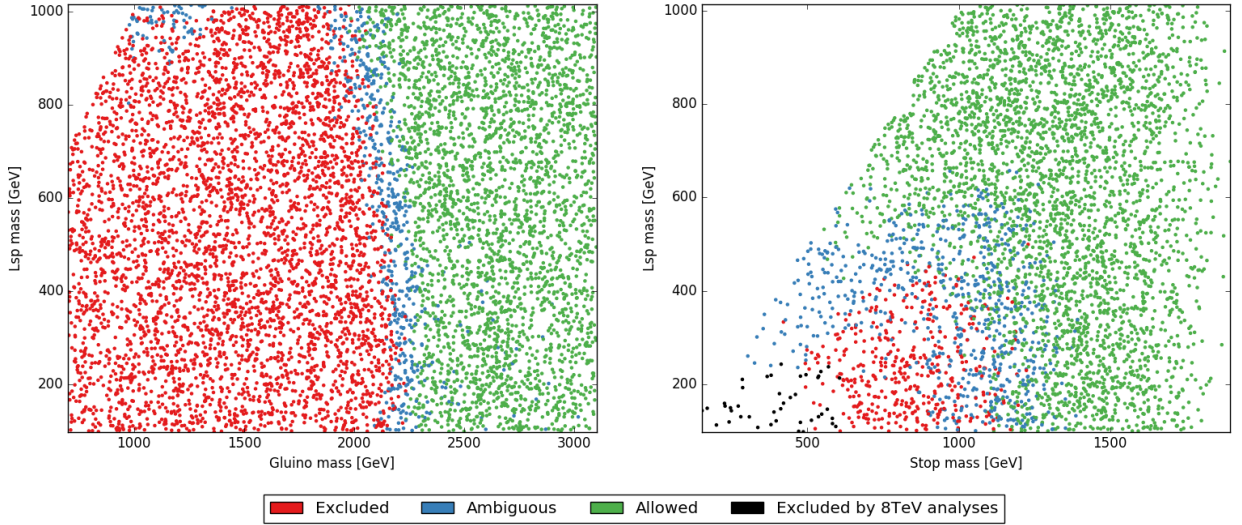


FIG. 7. Plots showing the natural SUSY points that are allowed, excluded or ambiguous within the Monte Carlo uncertainty at $\sqrt{s} = 14$ TeV with $\mathcal{L} = 300 \text{ fb}^{-1}$, under the assumption that the current systematic errors will remain constant. Left: $m_{\tilde{g}}$ vs $m_{\tilde{\chi}_1^0}$ for $m_{\tilde{t}_1} > 1300$ GeV. Right: $m_{\tilde{t}_1}$ vs $m_{\tilde{\chi}_1^0}$ for $m_{\tilde{g}} > 2500$ GeV.

In order to isolate the dependence of the LHC reach on the stop mass, we now have to place a far harder cut on the gluino mass ($m_{\tilde{g}} > 2500$ GeV) in our selection, and this leads to the sparser coverage of points shown in Fig. 7 (right). However, the plot still clearly shows the improved sensitivity to stop states, with masses above $m_{\tilde{t}_1} \sim 1200$ GeV now probed for direct production. Nonetheless, the coverage is not complete and much lighter stop states ($m_{\tilde{t}_1} < 1000$ GeV) are in the “ambiguous” category even with an LSP of $m_{\tilde{\chi}_1^0} \sim 100$ GeV.

D. Exclusion with 3000 fb^{-1} at 14 TeV

Further evolution in the bounds is seen as we move to the final luminosity estimates expected for the HL LHC, and these are shown in Fig. 8. We see that gluinos can now be excluded up to almost $m_{\tilde{g}} \sim 2500$ GeV for certain scenarios, and all points with $m_{\tilde{g}} < 2000$ GeV can definitely be excluded as long as the parameter points are not highly compressed. Even in the compressed region, however, we see very good coverage with almost all points at $m_{\tilde{\chi}_1^0} \sim m_{\tilde{g}} \sim 1000$ GeV completely excluded and only a few remain-

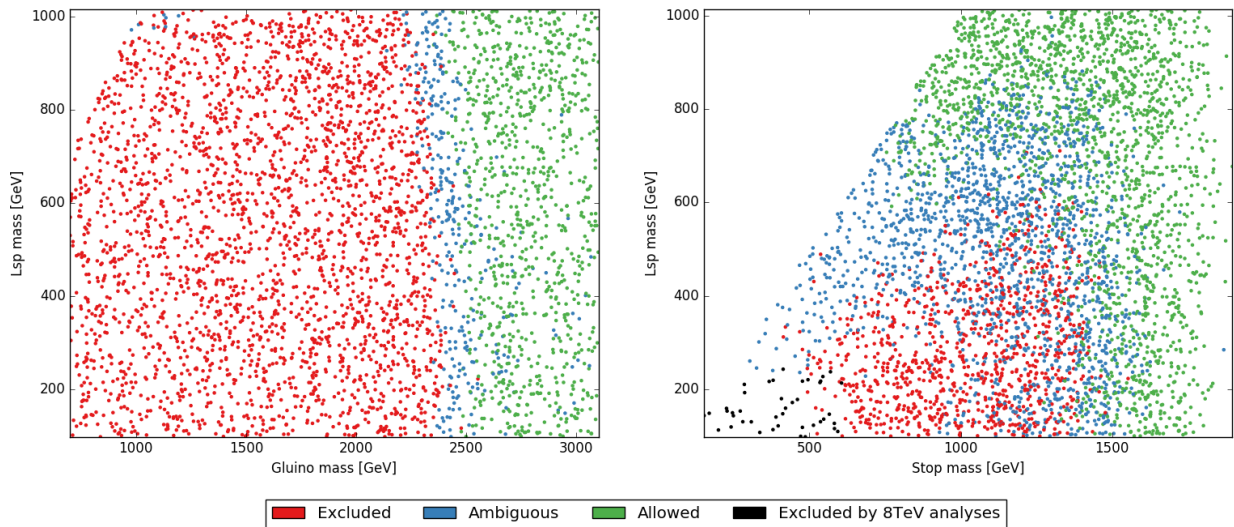


FIG. 8. Plots showing the natural SUSY points that are allowed, excluded or ambiguous within the Monte Carlo uncertainty at $\sqrt{s} = 14$ TeV with $\mathcal{L} = 3000 \text{ fb}^{-1}$, under the assumption that the current systematic errors will remain constant. Left: $m_{\tilde{g}}$ vs $m_{\tilde{\chi}_1^0}$ for $m_{\tilde{t}_1} > 1500$ GeV. Right: $m_{\tilde{t}_1}$ vs $m_{\tilde{\chi}_1^0}$ for $m_{\tilde{g}} > 2500$ GeV.

ing in the ambiguous category.

For stops the limits can now even reach beyond $m_{\tilde{t}_1} \sim 1500$ GeV for the most sensitive parameter points. However, we still see significant variation across the parameter space, and some models with a light stop with $m_{\tilde{t}_1} < 1000$ GeV are in the ambiguous category, which we cannot be sure will be excluded. Some of this variation is due to differences in how the stop states can decay but the major difference is down to the masses of the other coloured scalars in the theory.

For example, if we examine the ambiguous points in Fig. 8 (right) with $m_{\tilde{t}_1} < 1000$ GeV and $m_{\tilde{\chi}_1^0} \sim 100$ GeV, we find that the light stop in these parameter points is the right-handed SU(2) singlet. It decays at comparable rates to different final states (see Eqs. (4) and (5) and the following discussion), which weakens sensitivity of the individual searches. The SU(2)-doublet stop (along with the partner sbottom) by contrast is effectively decoupled from the LHC phenomenology with masses ~ 2000 GeV. In addition, the gluinos are very heavy for these points, with $m_{\tilde{g}} \sim 3000$ GeV.

A comparison to these light stop points is provided by a spectra where the lightest stop has $m_{\tilde{t}_1} \sim 1500$ GeV but the point can still be excluded. The reason is that all of the coloured scalars ($\tilde{t}_1, \tilde{t}_2, \tilde{b}_1$) in the model have a very similar mass (~ 1500 GeV), and this provides a significant production cross section. In addition, while the gluino is not light enough by itself to result in the parameter point being excluded, the mass ($m_{\tilde{g}} \sim 2560$ GeV) is in the borderline region, where the production cross section still provides additional events for the dedicated stop searches.

E. Exclusion with 3000 fb^{-1} at 14 TeV: Reduced errors

In all of the above results we have assumed that the systematic uncertainties are constant (as a proportion) for all the different luminosities and energies that we investigate. However, it can be expected that as the LHC develops, these uncertainties will reduce as the collider and detectors become better understood. In particular, many backgrounds do not rely on MC predictions but are derived from data, and thus the uncertainty can be expected to improve. As an approximation to illustrate how the reach of the LHC can improve as the uncertainties are reduced, we take the current errors at 20 fb^{-1} as the baseline and scale these according to the collected statistics (i.e. the uncertainties reduce $\propto 1/\sqrt{\mathcal{L}}$, see Sec. III C 3).

Figure 9 shows the expected parameter points that can be excluded, are ambiguous or are expected to be allowed under the above assumption. We see that for the gluino limits the effect is not so stark, and it simply increases the expected exclusion for almost all parameter points investigated to $m_{\tilde{g}} > 2500$ GeV.

The effect on the stop limits, however, is far stronger. Figure 9 (right) shows that the exclusion is possible for the majority of points with $m_{\tilde{t}_1} < 1400$ GeV and $m_{\tilde{\chi}_1^0} < 600$ GeV. This is a significant change compared to the scenario where the systematic errors remained unchanged and some points with $m_{\tilde{t}_1} \sim 900$ GeV were still not definitely excluded. In addition, in the region where the LSP is heavier and the scenario begins to become compressed the limits also increase substantially. For example, without a reduction in the systematic error, no strict bound on the LSP mass for $m_{\tilde{t}_1} \sim 1000$ GeV could be set. How-

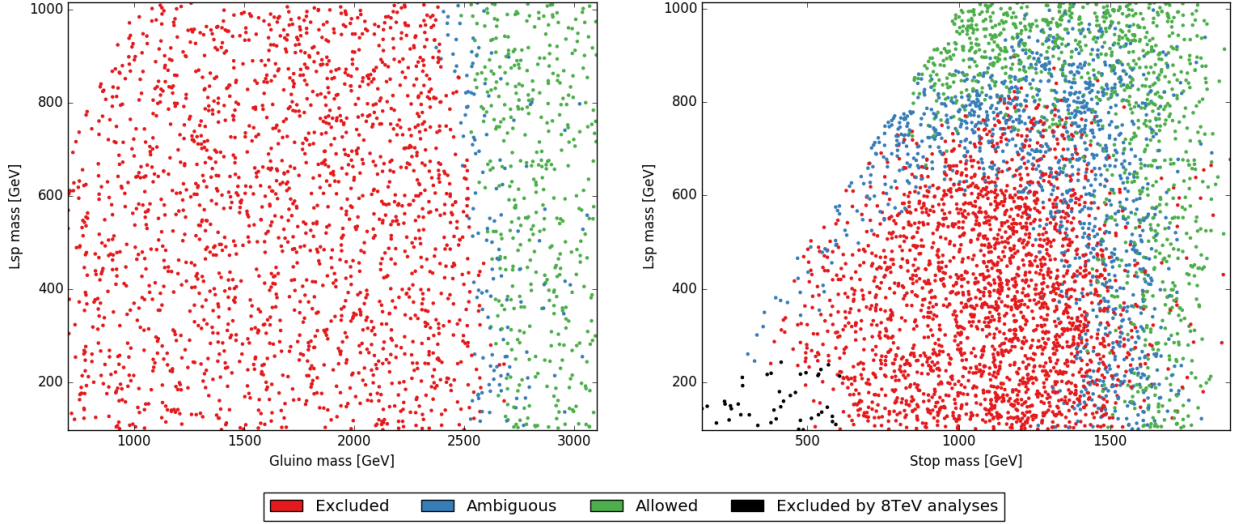


FIG. 9. Plots showing the natural SUSY points that are allowed, excluded or ambiguous within the Monte Carlo uncertainty at $\sqrt{s} = 14$ TeV with $\mathcal{L} = 3000 \text{ fb}^{-1}$, under the assumption that the systematic errors will reduce in proportion to the collected luminosity. Left: $m_{\tilde{g}}$ vs $m_{\tilde{\chi}_1^0}$ for $m_{\tilde{t}_1} > 1600$ GeV. Right: $m_{\tilde{t}_1}$ vs $m_{\tilde{\chi}_1^0}$ for $m_{\tilde{g}} > 2500$ GeV.

ever, with the reduced error we now find no parameter points that are allowed and only a few that are ambiguous for $m_{\tilde{t}_1} \sim 1000$ GeV with $m_{\tilde{\chi}_1^0} < 600$ GeV.

One may ask, why the reach to stop states is improved far more with reduced systematic uncertainties compared to the increase in the gluino limits. Our reasoning is that different kinematics are probed by high-mass gluino production compared to the lower mass stop production. Namely, the gluino searches are at the LHC kinematic limit when probing pair production with $m_{\tilde{g}} \sim 2500$ GeV. Here the parton distribution functions (PDFs) are dropping so quickly, even when we reduce the systematic errors significantly, that we simply lack enough signal events for the limits to increase appreciably.

The stop limits are different since for their typical masses (~ 1000 GeV), we are much further away from the kinematic boundary where the PDFs rapidly reduce the production cross sections. Rather, the difficulty in successfully setting limits is due to the large standard model background that comes predominantly from top pair production. If we can successfully reduce the systematic error on this background, far more of the parameter space can be probed.

F. Most sensitive analyses

In Fig. 10 we plot the most sensitive analysis for every parameter point that can be excluded with 3000 fb^{-1} at 14 TeV, assuming the systematic errors remain constant. We can clearly see that the parameter space can be divided into regions where different searches are most sensitive. If we first look at the $m_{\tilde{g}}$ vs $m_{\tilde{\chi}_1^0}$ plane (Fig. 10 (left)), we see that, in

general, the most powerful search for kinematically accessible gluinos ($m_{\tilde{g}} < 2300$ GeV) and light LSPs ($m_{\tilde{\chi}_1^0} \lesssim 600$ GeV) is the one-lepton stop pair production search [64] shown in blue. Since these points are dominated by gluino production, this may, at first sight, seem surprising. However, the signal regions are reasonably general and rely on the following:

- large missing energy, E_T^{miss} ;
- transverse mass between the lepton and E_T^{miss} ;
- E_T^{miss} significance, $E_T^{\text{miss}}/\sqrt{H_T}$, where $H_T = \sum_{\text{jets}=1}^4 |\vec{p}_T|$;
- reconstructed hadronic top, $130 < m_{jjj} < 205$ GeV.

Since the gluinos in our scenarios very commonly decay via cascades involving top quarks, it is easy to see why such an analysis is so sensitive to our models.

In similar regions of parameter space we also find that the 0-lepton version of the analysis [64] is sensitive (points in red). Again, this is not surprising because the search concentrates on high missing energy along with high jet multiplicity (≥ 6), of which at least two must be b -jets. While these signal regions are again labelled as stop searches we should point out that they actually share more in common with the current gluino searches, and thus it is natural that they so strongly constrain the gluinos in our model.

As we go to higher LSP masses ($m_{\tilde{\chi}_1^0} \gtrsim 600$ GeV), we see a bulk region in orange that denotes the parameter points expected to be excluded by the three b -jets search for gluinos [60]. The reason why the general gluino search becomes more sensitive in this region is that the spectrum starts to become more compressed

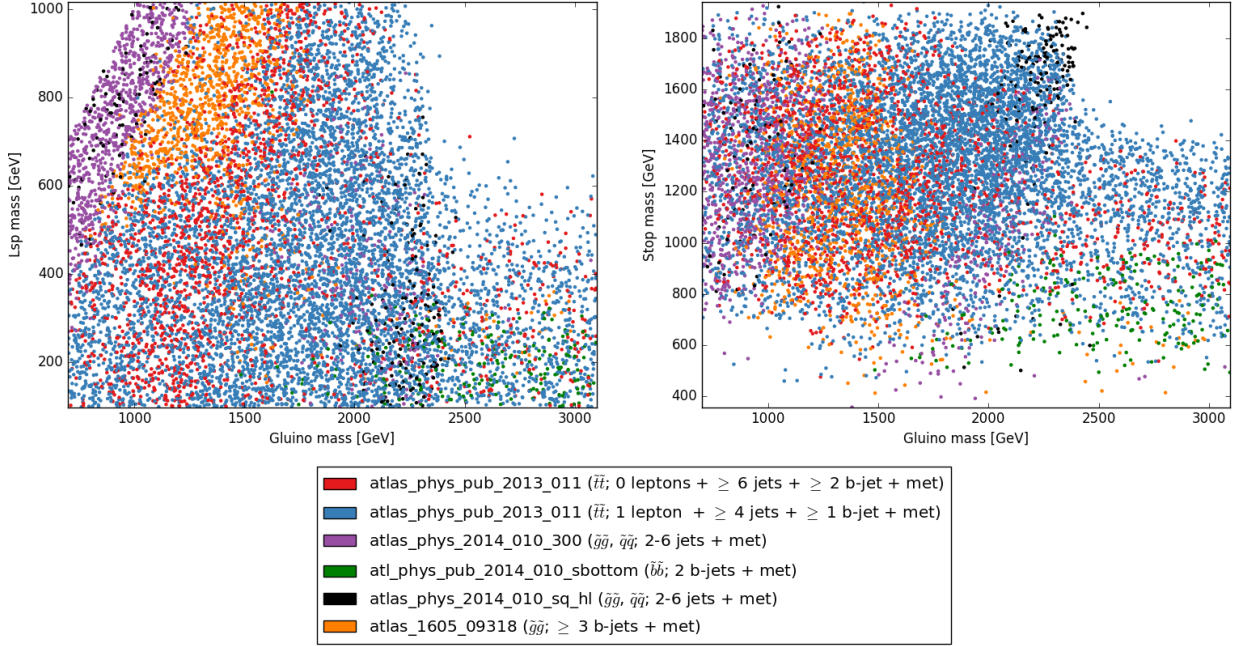


FIG. 10. Most constraining analyses for each of the parameter points excluded at $\sqrt{s} = 14\text{ TeV}$ with $\mathcal{L} = 3000\text{ fb}^{-1}$ assuming the systematic errors remain constant. Left: $m_{\tilde{g}}$ vs $m_{\tilde{\chi}_1^0}$. Right: $m_{\tilde{g}}$ vs $m_{\tilde{t}_1}$.

as the LSP mass is raised. The consequence of such compression is that we produce fewer (or no) on-shell top quarks in the cascade decay chains. Consequently, the one-lepton stop search that requires a hadronically reconstructed top quark is no longer so sensitive, and we rely on the simpler jet, b -jet and missing energy search.

To the left of the orange region is an area dominated by purple points that signify the general jets and missing energy squark and gluino search but with the signal regions optimised for 300 fb^{-1} . This is the compressed region of parameter space where the gluino and LSP lie close in mass. Thus, the decay products of the gluino become soft, and we rely on initial state radiation (ISR) in order to set limits on the model. Consequently, it is not so surprising that the dominant search in this region no longer relies on b -tags or leptons since these will, in general, be softer and less likely to pass the kinematic cuts. In addition it is not surprising that the 300 fb^{-1} version of the jets and E_T^{miss} analysis performs better than the one optimised for 3000 fb^{-1} . The reason is that the cuts are softer for 300 fb^{-1} signal regions, and thus the acceptance for the ISR signature is much higher.

One may also ask how monojet searches may perform in this region since they can give the strongest bounds for very compressed models. However, this is typically only the case for extreme compression ($< 20\text{ GeV}$ mass difference) [72, 73], and more recent studies suggest that the multijet search may actually give stronger constraints on gluino production as we move to 13 TeV [79].

A region where the 3000 fb^{-1} jets and E_T^{miss} analysis does provide some of the strictest limits is for high mass gluino pair production between 2000 and 2500 GeV (black points). The region can be more clearly seen in the $m_{\tilde{g}}$ vs $m_{\tilde{t}_1}$ plane of Fig. 10 (right) with the black points at high gluino and stop masses.

The same plot also more clearly illustrates the signal region dependence in the area of parameter space where stop production dominates. These points can be seen for $m_{\tilde{g}} \gtrsim 2300\text{ GeV}$, where the high gluino mass leads to a decoupling from the LHC phenomenology. Looking at the plot we can clearly see a difference in the most sensitive analysis for stop masses above and below $\sim 1000\text{ GeV}$. Above this mass, the dominant search is the dedicated stop analysis with either one lepton (blue points) or 0 leptons (red points) in the final state. Such a result should be expected as these searches have been precisely tuned for stop masses in this range.

The green points in Fig. 10 (right) also show that if the spectrum contains a light sbottom squark, this can be a sensitive production mode. Such a search is particularly important for natural SUSY since, as stated before, if the lightest stop in the spectrum is the $\text{SU}(2)$ partner, the corresponding $\text{SU}(2)$ sbottom must be close in mass. We see that for lower masses, the direct search for sbottoms may actually be more sensitive than those for stops.

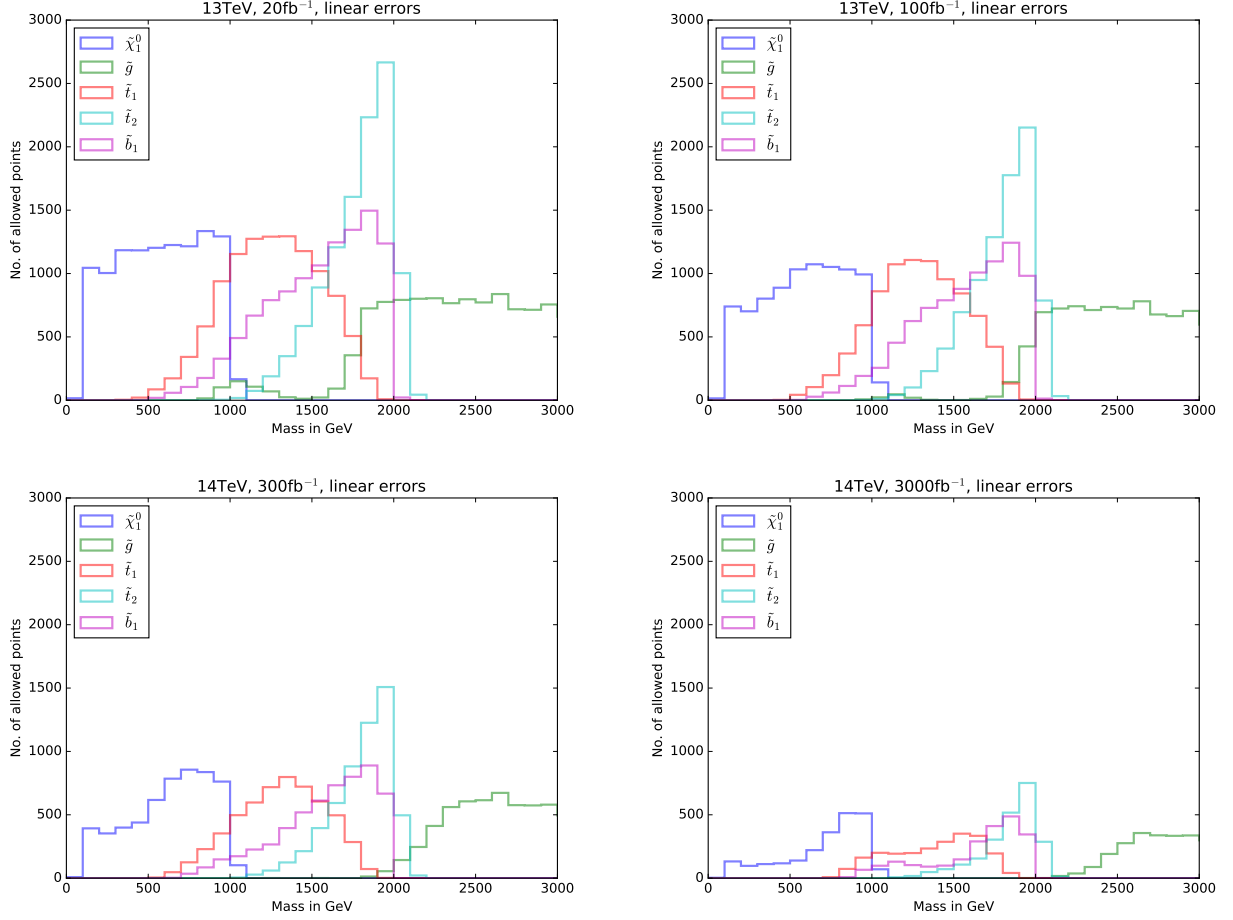


FIG. 11. Distribution of particle masses in allowed parameter points after 13 TeV with 20 fb⁻¹ (top left), 13 TeV with 100 fb⁻¹ (top right), 14 TeV with 300 fb⁻¹ (bottom left), 14 TeV with 3000 fb⁻¹ (bottom right).

G. Distribution of allowed points

The cumulative effect of the LHC searches at different energies and luminosities can be most easily seen by plotting distributions of the allowed mass spectra. We show these distributions in Fig. 11 for different integrated luminosity and energy stages.

It is instructive to start the analysis by comparing the distributions of all the analysed points, Fig. 4, to the distribution after 20 fb⁻¹ at $\sqrt{s} = 13$ TeV, the upper left panel of Fig. 11; we see that roughly half of the points become excluded at this stage. The distributions for stops and sbottoms have a similar shape, however, and this is due to the fact that the majority of the exclusion is driven by the mass of the gluino. For higgsinos we observe that the mass distribution is now skewed towards higher masses since compressed scenarios are more difficult to probe. The most dramatic change, however, can be seen for gluinos. The majority of the points with $m_{\tilde{g}} \lesssim 1900$ GeV would be excluded at this stage. This confirms the fact that gluinos offer the most robust discovery potential at the LHC.

As we continue the analysis for the following LHC stages we observe a rather modest improvement for $\sqrt{s} = 13$ TeV with 100 fb⁻¹, the upper right panel of Fig. 11. There is some reduction in the number of allowed points, of course, which is visible in the t_2 distribution. There is also a further shift towards heavier higgsinos. The trend continues for LHC 14 TeV with 300 fb⁻¹ (the lower left panel of Fig. 11), but we also observe an increase in the exclusion limit in the gluino masses, possibly more due to the increased centre-of-mass energy rather than the increased integrated luminosity.

At the final luminosity stage of 3000 fb⁻¹ (the lower right panel of Fig. 11), we see a clear difference in all distributions compared to Fig. 4. The allowed points now cumulate around upper limits of the scanning ranges, and the gluino exclusion limit is pushed to ~ 2500 GeV. Not surprisingly, however, there are still allowed points with low higgsino masses that would remain undetected as long as the other superpartners are sufficiently heavy.

H. Discovery with 3000 fb⁻¹ at 14 TeV

Of course, the focus of the LHC is not purely to exclude models of new physics but to hopefully actually discover new particles. For this reason, we also make projections for the discovery potential (5σ) of the HL LHC at 14 TeV with 3000 fb⁻¹. In Fig. 12 (left) we plot the points that can be discovered in the $m_{\tilde{g}}$ vs $m_{\tilde{\chi}_1^0}$ plane and colour these points according to whether they are predicted to be excluded, ambiguous or allowed with 20 fb⁻¹ at 13 TeV. The plot shows that gluinos up to ~ 2000 GeV can be discovered for light LSPs (the points beyond this are mainly due to light stops being present in the spectrum). As for the exclusion curves, discovery is much harder in the compressed region but can be made for some points up to $m_{\tilde{g}} \sim 1000$ GeV.

However, what is far more striking is that the vast majority of these points would have been excluded with 20 fb⁻¹ at 13 TeV. In fact only a very small proportion of points (in green) are definitely allowed with 20 fb⁻¹ at 13 TeV and these points lie in two distinct regions. First, there exists a thin strip, $1800 \lesssim m_{\tilde{g}} \lesssim 2100$ GeV where allowed points can be discovered. Second, in the region of high compression, the much higher statistics allows points to be discovered that were not excluded with 20 fb⁻¹ at 13 TeV. We therefore come to the conclusion that the coming LHC run will already begin to probe the majority of parameter points that contain a gluino within the eventual LHC discovery reach. Essentially, if natural SUSY is to be discovered at the LHC, we may expect the first signs to appear this year.

A very similar conclusion is reached if we examine the parameter points with light stop masses that can be discovered at the HL LHC. In Fig. 12 (right) we show the points that can be discovered in the $m_{\tilde{g}}$ vs $m_{\tilde{t}_1}$ plane. Here the majority of points with $m_{\tilde{g}} < 2000$ GeV are excluded by direct gluino searches, but beyond this, we see the parameter points that can be discovered thanks to direct stop production. We see that stop masses up to ~ 1200 GeV can be discovered in the natural SUSY paradigm. However, we also see that the majority of the points that can be discovered, will already have been excluded with 20 fb⁻¹ at 13 TeV. Once again, we see only a narrow strip (with some compressed spectra points below), this time in the range $800 \lesssim m_{\tilde{g}} \lesssim 1200$ GeV, which contains points that cannot be probed with 20 fb⁻¹ at 13 TeV but can be discovered. Therefore, for stops we also come to the conclusion that the first signs should appear soon if an unambiguous discovery can be made at the LHC.

I. Discovery with 3000 fb⁻¹ at 14 TeV: Reduced errors

The previous section makes the assumption that the systematic uncertainties on the background and signal remain at their current values. However, we also investigate how the discovery potential of the LHC is improved if the uncertainties can be reduced. We therefore again reduce the systematic uncertainties according to the increase in the collected statistics in the same way as Sec. IV E.

If we now compare the previously discussed discovery potential in Fig. 12 with the reduced uncertainty case shown in Fig. 13, we see a significant increase in the SUSY masses that the LHC can discover. Specifically, we see that in a natural SUSY setup we can expect to discover gluino masses up to $m_{\tilde{g}} \sim 2400$ GeV. Perhaps more importantly, however, is the fact that Fig. 13 (left) shows that the coverage for lighter gluinos ($m_{\tilde{g}} \lesssim 1500$ GeV) but heavier LSPs ($m_{\tilde{\chi}_1^0} \gtrsim 800$ GeV) is now far more comprehensive. Nevertheless, for the majority of these points, the first signs should already be seen at 13 TeV with 20 fb⁻¹.

A similar conclusion can also be reached when the discovery is facilitated by light top squarks in the spectrum. Examining Fig. 13 (right), we see that stops up to $m_{\tilde{t}_1} \sim 1400$ GeV can now be discovered, and this is to be compared to ~ 1200 GeV if the systematic errors are not reduced. As for the gluino case, however, the increase in the discovery potential is perhaps undersold by only studying the mass reach. More important is the fact that without reduced uncertainties, only a very small region of parameter space can be discovered with 3000 fb⁻¹ at 14 TeV that is not already ruled out with 20 fb⁻¹ at 13 TeV. If the uncertainties can be reduced, however, this picture changes significantly, and far more of the parameter space is left open for discovery.

V. SUMMARY AND CONCLUSION

In this paper we have examined the prospects of probing and even discovering so-called “natural” SUSY as the LHC progresses in both collected luminosity and energy. To map the progress we considered four different LHC scenarios: 20 fb⁻¹ at 13 TeV, 100 fb⁻¹ at 13 TeV, 300 fb⁻¹ at 14 TeV, and 3000 fb⁻¹ at 14 TeV, and first explored the gluino and lightest stop masses that can be excluded at each setup.

For gluino masses, the maximum exclusion ranges from ~ 1.7 TeV with 20 fb⁻¹ at 13 TeV to ~ 2.5 TeV with 3000 fb⁻¹ at 14 TeV. In contrast, the lower production cross sections for stops result in correspondingly weaker bounds of ~ 800 GeV with 20 fb⁻¹ at 13 TeV to ~ 1.5 TeV with 3000 fb⁻¹ at 14 TeV. We should also mention that these bounds heavily depend on the mass of the LSP in the spectrum. In particular,

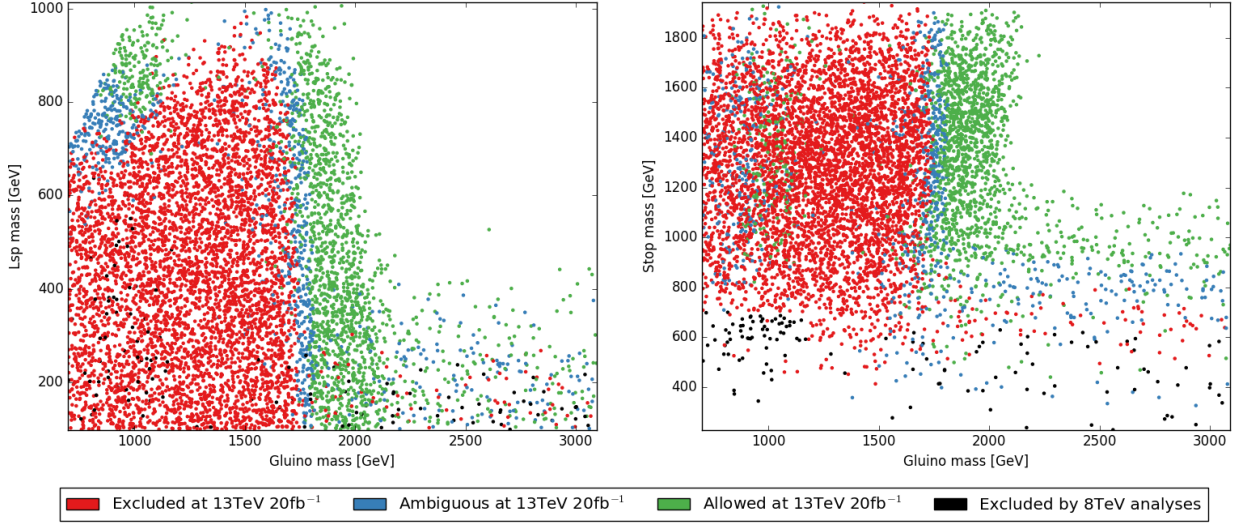


FIG. 12. Plots showing the natural SUSY points that can be discovered at $\sqrt{s} = 14$ TeV with $\mathcal{L} = 3000 \text{ fb}^{-1}$, under the assumption that the current systematic errors will remain constant. We classify these points as excluded, ambiguous within Monte Carlo uncertainty and allowed at 13 TeV with 20 fb^{-1} , and those already excluded at 8 TeV. Left: $m_{\tilde{g}}$ vs $m_{\tilde{\chi}_1^0}$. Right: $m_{\tilde{g}}$ vs $m_{\tilde{t}_1}$.

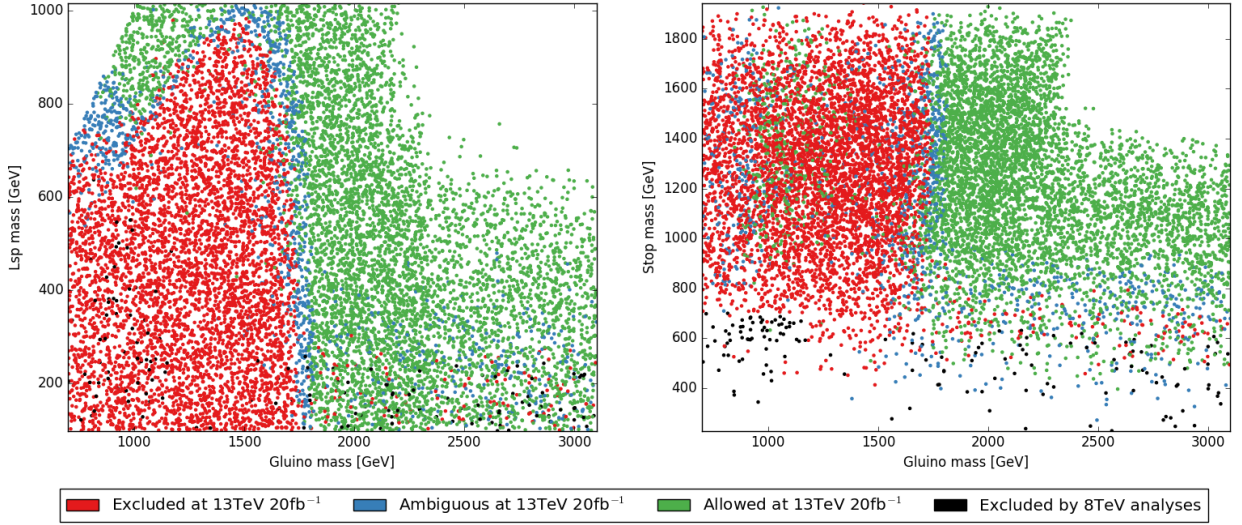


FIG. 13. Plots showing the natural SUSY points that can be discovered at $\sqrt{s} = 14$ TeV with $\mathcal{L} = 3000 \text{ fb}^{-1}$, under the assumption that the systematic errors will reduce in proportion to the collected luminosity. We classify these points as excluded, ambiguous within MC uncertainty and allowed at 13 TeV with 20 fb^{-1} , and those already excluded at 8 TeV. Left: $m_{\tilde{g}}$ vs $m_{\tilde{\chi}_1^0}$. Right: $m_{\tilde{g}}$ vs $m_{\tilde{t}_1}$.

as the LSP mass rises, the spectra become compressed, and we see a reduction in the LHC reach. For example, with 3000 fb^{-1} at 14 TeV we can set no bound on the stop mass if $\tilde{\chi}_1^0 \gtrsim 600$ GeV, but many points also survive with both lower stop and LSP masses.

The above conclusions assumed that the systematic uncertainties remain at approximately their current levels. In order to see how the LHC reach depends on this assumption, we also investigated the effect of reducing the systematic uncertainty according to

the collected luminosity (i.e. the uncertainty scales as $1/\sqrt{\mathcal{L}}$). Reducing the uncertainty in such a way only has a small effect on the LHC reach for gluinos, and the mass limits rise by ~ 100 GeV to $m_{\tilde{g}} \gtrsim 2600$. The small difference is due to the fact that for such high masses, gluino production is almost at the kinematic limit, and thus reduced systematic errors can only marginally improve the bound. In contrast, the limits on stop production are markedly improved. In particular, for low mass LSP stops can be reliably excluded

for $m_{\tilde{t}_1} < 1400$ GeV, whereas if the uncertainties remain constant, many points with $m_{\tilde{t}_1} \sim 1000$ GeV are ambiguous. A similar conclusion can be seen in terms of the LSP mass, where with the reduced errors, very few points with $m_{\tilde{\chi}_1^0} < 700$ GeV remain (assuming $m_{\tilde{t}_1} < 1400$ GeV). This can be compared to the case without reduced errors, where it is very hard to make strong statements in the $m_{\tilde{t}_1}$ vs $m_{\tilde{\chi}_1^0}$ plane.

Our most important results, however, are regarding the expected discovery reach of the LHC at high luminosity (3000 fb^{-1} at 14 TeV). We come to the rather sobering conclusion that assuming the systematic errors remain constant, there are relatively few parameter points that can be discovered that are not already excluded with 20 fb^{-1} at 13 TeV. Essentially, if natural SUSY is to be discovered at the LHC, the first hints probably need to start appearing this summer. The situation changes slightly if the systematic errors can be reduced as more data are collected at the LHC. If we again take the scenario that the systematic uncertainty scales as $1/\sqrt{\mathcal{L}}$, the prospects of a natural SUSY discovery at high luminosity become more optimistic. For gluinos we find a mass band $1800 \lesssim m_{\tilde{g}} \lesssim 2400$,

where spectra that are not excluded with 20 fb^{-1} at 13 TeV can still eventually be discovered. A similar mass band $900 \lesssim m_{\tilde{t}_1} \lesssim 1400$ exists for stops, and this shows the importance of reducing the systematic uncertainties to fully exploit the discovery potential of the high luminosity LHC.

ACKNOWLEDGMENTS

The authors thank Sascha Caron for useful discussions. The work of JSK has been partially supported by the MINECO, Spain, under Contract No. FPA2013-44773-P; Consolider-Ingenio CPAN CSD2007-00042 and the Spanish MINECO Centro de Excelencia Severo Ochoa Program under Grant No. SEV-2012-0249. JSK would like to thank the IBS CPTU in Daejeon for support and hospitality while part of this manuscript was prepared. KR is supported by the National Science Centre (Poland) under Grant No. 2015/19/D/ST2/03136.

-
- [1] **ATLAS** Collaboration, G. Aad *et al.*, “Summary of the ATLAS experiment’s sensitivity to supersymmetry after LHC Run 1 — interpreted in the phenomenological MSSM,” *JHEP* **10** (2015) 134, [arXiv:1508.06608 \[hep-ex\]](#).
 - [2] **CMS** Collaboration, V. Khachatryan *et al.*, “Phenomenological MSSM interpretation of CMS searches in pp collisions at $\sqrt{s} = 7$ and 8 TeV,” *JHEP* **10** (2016) 129, [arXiv:1606.03577 \[hep-ex\]](#).
 - [3] **ATLAS** Collaboration, G. Aad *et al.*, “ATLAS Run 1 searches for direct pair production of third-generation squarks at the Large Hadron Collider,” *Eur. Phys. J.* **C75** (2015) no. 10, 510, [arXiv:1506.08616 \[hep-ex\]](#). [Erratum: *Eur. Phys. J.* **C76**, no. 3, 153 (2016)].
 - [4] **ATLAS** Collaboration, G. Aad *et al.*, “Summary of the searches for squarks and gluinos using $\sqrt{s} = 8$ TeV pp collisions with the ATLAS experiment at the LHC,” *JHEP* **10** (2015) 054, [arXiv:1507.05525 \[hep-ex\]](#).
 - [5] **CMS** Collaboration, S. Chatrchyan *et al.*, “Search for supersymmetry in pp collisions at $\sqrt{s} = 8$ TeV in events with a single lepton, large jet multiplicity, and multiple b jets,” *Phys. Lett.* **B733** (2014) 328–353, [arXiv:1311.4937 \[hep-ex\]](#).
 - [6] **CMS** Collaboration, V. Khachatryan *et al.*, “Search for direct pair production of supersymmetric top quarks decaying to all-hadronic final states in pp collisions at $\sqrt{s} = 8$ TeV,” *Eur. Phys. J.* **C76** (2016) no. 8, 460, [arXiv:1603.00765 \[hep-ex\]](#).
 - [7] A. H. Chamseddine, R. L. Arnowitt, and P. Nath, “Locally Supersymmetric Grand Unification,” *Phys. Rev. Lett.* **49** (1982) 970.
 - [8] J. L. Feng, K. T. Matchev, and T. Moroi, “Multi - TeV scalars are natural in minimal supergravity,” *Phys. Rev. Lett.* **84** (2000) 2322–2325, [arXiv:hep-ph/9908309 \[hep-ph\]](#).
 - [9] R. Kitano and Y. Nomura, “Supersymmetry, naturalness, and signatures at the LHC,” *Phys. Rev.* **D73** (2006) 095004, [arXiv:hep-ph/0602096 \[hep-ph\]](#).
 - [10] H. Baer, V. Barger, P. Huang, and X. Tata, “Natural Supersymmetry: LHC, dark matter and ILC searches,” *JHEP* **05** (2012) 109, [arXiv:1203.5539 \[hep-ph\]](#).
 - [11] H. Baer, V. Barger, and P. Huang, “Hidden SUSY at the LHC: the light higgsino-world scenario and the role of a lepton collider,” *JHEP* **11** (2011) 031, [arXiv:1107.5581 \[hep-ph\]](#).
 - [12] M. Papucci, J. T. Ruderman, and A. Weiler, “Natural SUSY Endures,” *JHEP* **1209** (2012) 035, [arXiv:1110.6926 \[hep-ph\]](#).
 - [13] R. Barbieri and G. Giudice, “Upper bounds on supersymmetric particle masses,” *Nuclear Physics B* **306** (1988) no. 1, 63 – 76. <http://www.sciencedirect.com/science/article/pii/055032138890171X>.
 - [14] J. R. Ellis, K. Enqvist, D. V. Nanopoulos, and F. Zwirner, “Observables in Low-Energy Superstring Models,” *Mod. Phys. Lett.* **A01** (1986) 57.
 - [15] J. A. Casas, J. M. Moreno, S. Robles, K. Rolbiecki, and B. Zaldivar, “What is a Natural SUSY scenario?,” *JHEP* **06** (2015) 070, [arXiv:1407.6966 \[hep-ph\]](#).
 - [16] C. Han, K.-i. Hikasa, L. Wu, J. M. Yang, and Y. Zhang, “Current experimental bounds on stop mass in natural SUSY,” *JHEP* **10** (2013) 216, [arXiv:1308.5307 \[hep-ph\]](#).
 - [17] K. Kowalska and E. M. Sessolo, “Natural MSSM after the LHC 8 TeV run,” *Phys. Rev.* **D88** (2013)

- no. 7, 075001, [arXiv:1307.5790 \[hep-ph\]](#).
- [18] O. Buchmueller and J. Marrouche, “Universal mass limits on gluino and third-generation squarks in the context of Natural-like SUSY spectra,” *Int. J. Mod. Phys. A* **29** (2014) no. 06, 1450032, [arXiv:1304.2185 \[hep-ph\]](#).
- [19] G. Belanger, D. Ghosh, R. Godbole, and S. Kulkarni, “Light stop in the MSSM after LHC Run 1,” *JHEP* **09** (2015) 214, [arXiv:1506.00665 \[hep-ph\]](#).
- [20] A. Kobakhidze, N. Liu, L. Wu, J. M. Yang, and M. Zhang, “Closing up a light stop window in natural SUSY at LHC,” *Phys. Lett. B* **755** (2016) 76–81, [arXiv:1511.02371 \[hep-ph\]](#).
- [21] J. S. Kim, D. Schmeier, and J. Tattersall, “Role of the ‘N’ in the natural NMSSM for the LHC,” *Phys. Rev. D* **93** (2016) no. 5, 055018, [arXiv:1510.04871 \[hep-ph\]](#).
- [22] M. Drees and J. S. Kim, “Minimal natural supersymmetry after the LHC8,” *Phys. Rev. D* **93** (2016) no. 9, 095005, [arXiv:1511.04461 \[hep-ph\]](#).
- [23] ATLAS, CMS Collaboration, G. Aad *et al.*, “Combined Measurement of the Higgs Boson Mass in pp Collisions at $\sqrt{s} = 7$ and 8 TeV with the ATLAS and CMS Experiments,” *Phys. Rev. Lett.* **114** (2015) 191803, [arXiv:1503.07589 \[hep-ex\]](#).
- [24] P. Bechtle, S. Heinemeyer, O. Stal, T. Stefaniak, G. Weiglein, and L. Zeune, “MSSM Interpretations of the LHC Discovery: Light or Heavy Higgs?,” *Eur. Phys. J. C* **73** (2013) no. 4, 2354, [arXiv:1211.1955 \[hep-ph\]](#).
- [25] J. Wenniger, “LHC operation in 2015 and prospects for the future.” Moriond - La Thuile, 2016. <https://indico.in2p3.fr/event/12279/session/7/contribution/118/material/slides/0.pdf>.
- [26] “LHC commissioning schedule.” <http://lhccommissioning.web.cern.ch/lhccommissioning/schedule/LHC-schedule-update.pdf>. [Online; accessed 20-May-2016].
- [27] L. E. Ibanez and G. G. Ross, “Discrete gauge symmetries and the origin of baryon and lepton number conservation in supersymmetric versions of the standard model,” *Nucl. Phys. B* **368** (1992) 3–37.
- [28] M. Drees, H. Dreiner, D. Schmeier, J. Tattersall, and J. S. Kim, “CheckMATE: Confronting your Favourite New Physics Model with LHC Data,” *Comput. Phys. Commun.* **187** (2015) 227–265, [arXiv:1312.2591 \[hep-ph\]](#).
- [29] DELPHES 3 Collaboration, J. de Favereau *et al.*, “DELPHES 3, A modular framework for fast simulation of a generic collider experiment,” *JHEP* **1402** (2014) 057, [arXiv:1307.6346 \[hep-ex\]](#).
- [30] “The LEP SUSY Working Group and the ALEPH, DELPHI, L3 and OPAL experiments, note LEPSUSYWG/01-03.1.” <http://lepsusy.web.cern.ch/lepsusy>.
- [31] G. G. Ross, K. Schmidt-Hoberg, and F. Staub, “On the MSSM Higgsino mass and fine tuning,” *Phys. Lett. B* **759** (2016) 110–114, [arXiv:1603.09347 \[hep-ph\]](#).
- [32] J. S. Kim, O. Lebedev, and D. Schmeier, “Higgsophilic gauge bosons and monojets at the LHC,” *JHEP* **11** (2015) 128, [arXiv:1507.08673 \[hep-ph\]](#).
- [33] H. Baer, A. Mustafayev, and X. Tata, “Monojets and monophotons from light higgsino pair production at lhcl4,” *Phys. Rev. D* **89** (Mar, 2014) 055007. <http://link.aps.org/doi/10.1103/PhysRevD.89.055007>.
- [34] K. Rolbiecki, J. Tattersall, and G. Moortgat-Pick, “Towards Measuring the Stop Mixing Angle at the LHC,” *Eur. Phys. J. C* **71** (2011) 1517, [arXiv:0909.3196 \[hep-ph\]](#).
- [35] K.-i. Hikasa and M. Kobayashi, “Light Scalar Top at e^+e^- Colliders,” *Phys. Rev. D* **36** (1987) 724.
- [36] H. Baer, X. Tata, and J. Woodside, “Phenomenology of Gluino Decays via Loops and Top Quark Yukawa Coupling,” *Phys. Rev. D* **42** (1990) 1568–1576.
- [37] W. Porod and F. Staub, “SPHeno 3.1: Extensions including flavour, CP-phases and models beyond the MSSM,” *Comput. Phys. Commun.* **183** (2012) 2458–2469, [arXiv:1104.1573 \[hep-ph\]](#).
- [38] T. Sjöstrand, S. Ask, J. R. Christiansen, R. Corke, N. Desai, P. Ilten, S. Mrenna, S. Prestel, C. O. Rasmussen, and P. Z. Skands, “An Introduction to PYTHIA 8.2,” *Comput. Phys. Commun.* **191** (2015) 159–177, [arXiv:1410.3012 \[hep-ph\]](#).
- [39] N. Desai and P. Z. Skands, “Supersymmetry and Generic BSM Models in PYTHIA 8,” *Eur. Phys. J. C* **72** (2012) 2238, [arXiv:1109.5852 \[hep-ph\]](#).
- [40] P. M. Nadolsky, H.-L. Lai, Q.-H. Cao, J. Huston, J. Pumplin, D. Stump, W.-K. Tung, and C. P. Yuan, “Implications of CTEQ global analysis for collider observables,” *Phys. Rev. D* **78** (2008) 013004, [arXiv:0802.0007 \[hep-ph\]](#).
- [41] W. Beenakker, R. Hopker, M. Spira, and P. Zerwas, “Squark and gluino production at hadron colliders,” *Nucl. Phys. B* **492** (1997) 51–103, [arXiv:hep-ph/9610490 \[hep-ph\]](#).
- [42] W. Beenakker, M. Kramer, T. Plehn, M. Spira, and P. Zerwas, “Stop production at hadron colliders,” *Nucl. Phys. B* **515** (1998) 3–14, [arXiv:hep-ph/9710451 \[hep-ph\]](#).
- [43] A. Kulesza and L. Motyka, “Threshold resummation for squark-antisquark and gluino-pair production at the LHC,” *Phys. Rev. Lett.* **102** (2009) 111802, [arXiv:0807.2405 \[hep-ph\]](#).
- [44] A. Kulesza and L. Motyka, “Soft gluon resummation for the production of gluino-gluino and squark-antisquark pairs at the LHC,” *Phys. Rev. D* **80** (2009) 095004, [arXiv:0905.4749 \[hep-ph\]](#).
- [45] W. Beenakker, S. Brensing, M. Kramer, A. Kulesza, E. Laenen, *et al.*, “Supersymmetric top and bottom squark production at hadron colliders,” *JHEP* **1008** (2010) 098, [arXiv:1006.4771 \[hep-ph\]](#).
- [46] W. Beenakker, S. Brensing, M. Kramer, A. Kulesza, E. Laenen, *et al.*, “Squark and Gluino Hadroproduction,” *Int. J. Mod. Phys. A* **26** (2011) 2637–2664, [arXiv:1105.1110 \[hep-ph\]](#).
- [47] J. S. Kim, D. Schmeier, J. Tattersall, and K. Rolbiecki, “A framework to create customised LHC analyses within CheckMATE,” *Comput. Phys. Commun.* **196** (2015) 535–562, [arXiv:1503.01123 \[hep-ph\]](#).
- [48] <http://checkmate.hepforge.org/>.
- [49] M. Cacciari and G. P. Salam, “Dispelling the N^3 myth for the k_t jet-finder,” *Phys. Lett. B* **641** (2006) 57–61, [arXiv:hep-ph/0512210 \[hep-ph\]](#).
- [50] M. Cacciari, G. P. Salam, and G. Soyez, “The Anti- k_t jet clustering algorithm,” *JHEP* **0804** (2008) 063, [arXiv:0802.1189 \[hep-ph\]](#).

- [51] M. Cacciari, G. P. Salam, and G. Soyez, “FastJet User Manual,” *Eur.Phys.J.* **C72** (2012) 1896, [arXiv:1111.6097 \[hep-ph\]](#).
- [52] M. Drees and K. Hagiwara, “Supersymmetric Contribution to the Electroweak ρ Parameter,” *Phys. Rev.* **D42** (1990) 1709–1725.
- [53] **Heavy Flavor Averaging Group** Collaboration, Y. Amhis *et al.*, “Averages of B-Hadron, C-Hadron, and tau-lepton properties as of early 2012,” [arXiv:1207.1158 \[hep-ex\]](#).
- [54] **OPAL** Collaboration, G. Abbiendi *et al.*, “Search for nearly mass degenerate charginos and neutralinos at LEP,” *Eur. Phys. J.* **C29** (2003) 479–489, [arXiv:hep-ex/0210043 \[hep-ex\]](#).
- [55] **DELPHI** Collaboration, J. Abdallah *et al.*, “Searches for supersymmetric particles in e^+e^- collisions up to 208 GeV and interpretation of the results within the MSSM,” *Eur. Phys. J.* **C31** (2003) 421–479, [arXiv:hep-ex/0311019 \[hep-ex\]](#).
- [56] **OPAL** Collaboration, G. Abbiendi *et al.*, “Search for chargino and neutralino production at $\sqrt{s} = 192$ GeV to 209 GeV at LEP,” *Eur. Phys. J.* **C35** (2004) 1–20, [arXiv:hep-ex/0401026 \[hep-ex\]](#).
- [57] J. Bramante, P. J. Fox, A. Martin, B. Ostdiek, T. Plehn, T. Schell, and M. Takeuchi, “Relic neutralino surface at a 100 TeV collider,” *Phys. Rev.* **D91** (2015) 054015, [arXiv:1412.4789 \[hep-ph\]](#).
- [58] C. Boehm, A. Djouadi, and M. Drees, “Light scalar top quarks and supersymmetric dark matter,” *Phys. Rev.* **D62** (2000) 035012, [arXiv:hep-ph/9911496 \[hep-ph\]](#).
- [59] J. S. Kim and T. S. Ray, “The higgsino-singlino world at the large hadron collider,” *Eur. Phys. J.* **C75** (2015) 40, [arXiv:1405.3700 \[hep-ph\]](#).
- [60] **ATLAS** Collaboration, “Search for pair-production of gluinos decaying via stop and sbottom in events with b -jets and large missing transverse momentum in $\sqrt{s} = 13$ TeV pp collisions with the ATLAS detector,” Tech. Rep. ATLAS-CONF-2015-067, CERN, Geneva, Dec, 2015. <http://cds.cern.ch/record/2114839>.
- [61] A. L. Read, “Presentation of search results: The CL(s) technique,” *J. Phys.* **G28** (2002) 2693–2704.
- [62] J. T. Linnemann, “Measures of significance in HEP and astrophysics,” *eConf* **C030908** (2003) MOBT001, [arXiv:physics/0312059 \[physics.data-an\]](#).
- [63] **ATLAS** Collaboration, “Search for Supersymmetry at the high luminosity LHC with the ATLAS experiment,” Tech. Rep. ATL-PHYS-PUB-2014-010, CERN, Geneva, Jul, 2014. <http://cds.cern.ch/record/1735031>.
- [64] **ATLAS** Collaboration, “Prospects for benchmark Supersymmetry searches at the high luminosity LHC with the ATLAS Detector,” Tech. Rep. ATL-PHYS-PUB-2013-011, CERN, Geneva, Sep, 2013. <http://cds.cern.ch/record/1604505>.
- [65] J. Alwall, M. Herquet, F. Maltoni, O. Mattelaer, and T. Stelzer, “MadGraph 5 : Going Beyond,” *JHEP* **06** (2011) 128, [arXiv:1106.0522 \[hep-ph\]](#).
- [66] J. Alwall, R. Frederix, S. Frixione, V. Hirschi, F. Maltoni, O. Mattelaer, H. S. Shao, T. Stelzer, P. Torrielli, and M. Zaro, “The automated computation of tree-level and next-to-leading order differential cross sections, and their matching to parton shower simulations,” *JHEP* **07** (2014) 079, [arXiv:1405.0301 \[hep-ph\]](#).
- [67] **ATLAS** Collaboration, G. Aad *et al.*, “Search for new phenomena in final states with an energetic jet and large missing transverse momentum in pp collisions at $\sqrt{s} = 8$ TeV with the ATLAS detector,” *Eur. Phys. J.* **C75** (2015) no. 7, 299, [arXiv:1502.01518 \[hep-ex\]](#). [Erratum: *Eur. Phys. J.* **C75**, no. 9, 408 (2015)].
- [68] **ATLAS** Collaboration, G. Aad *et al.*, “Search for direct third-generation squark pair production in final states with missing transverse momentum and two b -jets in $\sqrt{s} = 8$ TeV pp collisions with the ATLAS detector,” *JHEP* **1310** (2013) 189, [arXiv:1308.2631 \[hep-ex\]](#).
- [69] **ATLAS** Collaboration, G. Aad *et al.*, “Search for squarks and gluinos with the ATLAS detector in final states with jets and missing transverse momentum using $\sqrt{s} = 8$ TeV proton–proton collision data,” *JHEP* **09** (2014) 176, [arXiv:1405.7875 \[hep-ex\]](#).
- [70] **ATLAS** Collaboration, G. Aad *et al.*, “Search for strong production of supersymmetric particles in final states with missing transverse momentum and at least three b -jets at $\sqrt{s} = 8$ TeV proton-proton collisions with the ATLAS detector,” *JHEP* **10** (2014) 024, [arXiv:1407.0600 \[hep-ex\]](#).
- [71] T. J. LeCompte and S. P. Martin, “Large Hadron Collider reach for supersymmetric models with compressed mass spectra,” *Phys. Rev.* **D84** (2011) 015004, [arXiv:1105.4304 \[hep-ph\]](#).
- [72] H. K. Dreiner, M. Kramer, and J. Tattersall, “How low can SUSY go? Matching, monojets and compressed spectra,” *Europhys. Lett.* **99** (2012) 61001, [arXiv:1207.1613 \[hep-ph\]](#).
- [73] H. Dreiner, M. Kramer, and J. Tattersall, “Exploring QCD uncertainties when setting limits on compressed supersymmetric spectra,” *Phys. Rev.* **D87** (2013) no. 3, 035006, [arXiv:1211.4981 \[hep-ph\]](#).
- [74] M. Carena, A. Freitas, and C. E. M. Wagner, “Light Stop Searches at the LHC in Events with One Hard Photon or Jet and Missing Energy,” *JHEP* **10** (2008) 109, [arXiv:0808.2298 \[hep-ph\]](#).
- [75] M. Drees, M. Hanussek, and J. S. Kim, “Light Stop Searches at the LHC with Monojet Events,” *Phys. Rev.* **D86** (2012) 035024, [arXiv:1201.5714 \[hep-ph\]](#).
- [76] S. Bornhauser, M. Drees, S. Grab, and J. S. Kim, “Light Stop Searches at the LHC in Events with two b -Jets and Missing Energy,” *Phys. Rev.* **D83** (2011) 035008, [arXiv:1011.5508 \[hep-ph\]](#).
- [77] G. Hiller, J. S. Kim, and H. Sedello, “Collider Signatures of Minimal Flavor Mixing from Stop Decay Length Measurements,” *Phys. Rev.* **D80** (2009) 115016, [arXiv:0910.2124 \[hep-ph\]](#).
- [78] **ATLAS** Collaboration, G. Aad *et al.*, “Search for long-lived stopped R-hadrons decaying out-of-time with pp collisions using the ATLAS detector,” *Phys. Rev.* **D88** (2013) no. 11, 112003, [arXiv:1310.6584 \[hep-ex\]](#).
- [79] G. Chalons and D. Sengupta, “Closing in on compressed gluino-neutralino spectra at the LHC,” *JHEP* **12** (2015) 129, [arXiv:1508.06735 \[hep-ph\]](#).